iScience

CellPress

Article

Mesenchymal-Epithelial Interactome Analysis Reveals Essential Factors Required for Fibroblast-Free Alveolosphere Formation

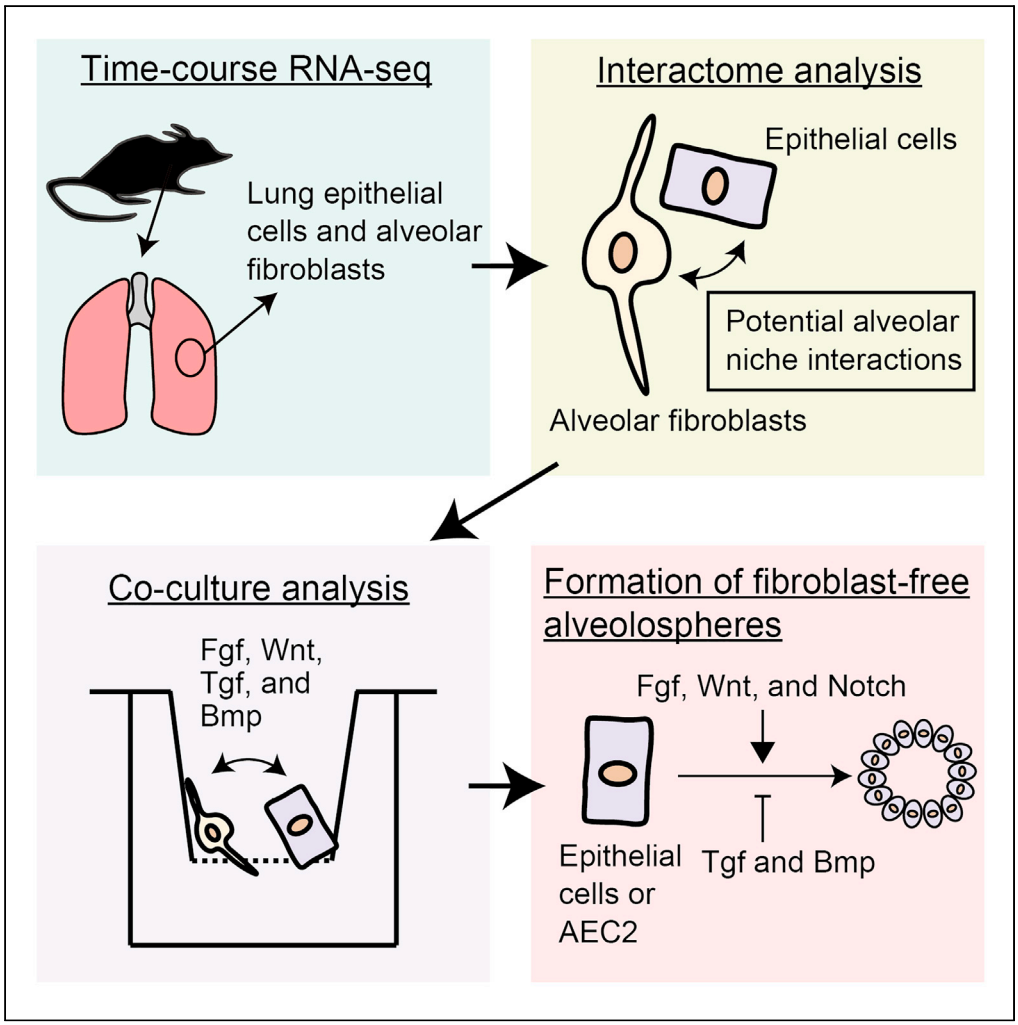

Kazushige Shiraishi, Shigeyuki Shichino, Satoshi Ueha, Takuya Nakajima, Shinichi Hashimoto, Satoshi Yamazaki, Kouji Matsushima

koujim@rs.tus.ac.jp

HIGHLIGHTS

Lung fibroblast-epithelial interactions regulating alveologenesis were analyzed

The interactions were assessed in fibroblast-epithelial co-culture organoid assays

A specific combination of molecules enabled fibroblast-free alveolosphere formation

The spheres were passageable and could be used to study lung development and biology

DATA AND SOFTWARE AVAILABILITY

GSE113160
GSE109847

Shiraishi et al., iScience *11*, 318–333
January 25, 2019
https://doi.org/10.1016/j.isci.2018.12.022

iScience

CellPress

Article

Mesenchymal-Epithelial Interactome Analysis Reveals Essential Factors Required for Fibroblast-Free Alveolosphere Formation

Kazushige Shiraishi,[1,2] Shigeyuki Shichino,[1,2] Satoshi Ueha,[1,2] Takuya Nakajima,[1,2] Shinichi Hashimoto,[1,2,3] Satoshi Yamazaki,[4] and Kouji Matsushima[1,2,5,*]

SUMMARY

Lung epithelial cells and fibroblasts are key cell populations in lung development. Fibroblasts support type 2 alveolar epithelial cells (AEC2) in the developing and mature lung. However, fibroblast-AEC2 interactions have not been clearly described. We addressed this in the present study by time course serial analysis of gene expression sequencing (SAGE-seq) of epithelial cells and fibroblasts of developing and mature murine lungs. We identified lung fibroblast-epithelial interactions that potentially regulate alveologenesis and are mediated by fibroblast-expressed ligands and epithelial cell surface receptors. In the epithelial-fibroblast co-culture alveolosphere formation assay, single intervention against fibroblast-expressed ligand or associated signaling cascades promoted or inhibited alveolosphere growth. Adding the ligand-associated molecules fibroblast growth factor 7 and Notch ligand and inhibitors of bone morphogenetic protein 4, transforming growth factor β, and glycogen synthase kinase-3β to the culture medium enabled fibroblast-free alveolosphere formation. The results revealed the essential factors regulating fibroblast-AEC2 interactions.

INTRODUCTION

The lungs consist of at least 40–60 different cell types that form a complex three-dimensional structure, with branched epithelial walls surrounded by interstitium and a vascular network (McQualter and Bertoncello, 2012). The airway epithelium is composed of ciliated, secretory (club and goblet), and basal cells (Barkauskas et al., 2017). In contrast, the alveolar epithelium where gas exchange takes place comprises two cell types—type 2 alveolar epithelial cells (AEC2) that secrete surfactant proteins and are considered as tissue stem cells and type 1 alveolar epithelial cells (AEC1) that form a thin wall for gas exchange (Barkauskas et al., 2013). In alveoli, fibroblasts are in close contact with and are thought to support AEC2 maintenance, constituting an alveolar stem cell niche (Hogan et al., 2014).

Lung development begins at around embryonic day 9.0 (E9.0) in mice, and maturation of alveoli starts at around E16.5 and continues to around postnatal day 30 (P30) (Herriges and Morrisey, 2014). In the developing and mature lung, fibroblasts interact with and support the differentiation and maturation of epithelial cells (McCulley et al., 2015); thus, fibroblast-epithelial cell interactions are important in alveologenesis and AEC2 maintenance. Indeed, alveolospheres—an organoid derived from AEC2—can be generated by co-culturing AEC2 with lung mesenchymal cells (Barkauskas et al., 2013); alveolosphere cultures have been used to investigate fibroblast-AEC2 interactions *in vitro* (Zepp et al., 2017). However, the molecular mechanisms of fibroblast-AEC2 interactions and the factors critical for alveolosphere formation are not known.

To investigate fibroblast-AEC2 interactions, we carried out a time course serial analysis of gene expression sequencing (SAGE-seq) of lung epithelial cells and fibroblasts during alveologenesis and in the mature state. We demonstrate that these interactions are mediated by pairs of fibroblast ligands and their cognate epithelial receptors. Moreover, the results of our *in vitro* alveolosphere formation assay revealed a set of ligand-associated factors that are required for fibroblast-free alveolosphere formation.

RESULTS

Transcriptional Changes during Alveologenesis and in Mature Lungs

To clarify fibroblast-epithelial interactions during alveologenesis and in mature lungs, we performed a time course transcriptome analysis of epithelial cells and fibroblasts in developing and mature murine lungs. We

[1]Department of Molecular Preventive Medicine, Graduate School of Medicine, The University of Tokyo, Tokyo 113-0033, Japan

[2]Division of Molecular Regulation of Inflammatory and Immune Diseases, Research Institute of Biomedical Sciences, Tokyo University of Science, Noda 278-0022, Japan

[3]Department of Integrative Medicine for Longevity, Graduate School of Medical Sciences, Kanazawa University, Kanazawa 920-8641, Japan

[4]Division of Stem Cell Therapy, Center for Stem Cell Biology and Regenerative Medicine, The Institute of Medical Science, The University of Tokyo, Tokyo 108-8639, Japan

[5]Lead Contact

*Correspondence: koujim@rs.tus.ac.jp

https://doi.org/10.1016/j.isci.2018.12.022

purified lineage (CD31, CD45, CD146 and Ter119)$^-$ Epcam$^+$ lung epithelial cells and lineage$^-$ GFP$^+$ fibroblasts from E18.5, P0.5, P2, P7, P28, and P56 (fibroblasts only) Col1a2-GFP mice for SAGE-seq analysis (Figures 1A and 1B). We performed flow cytometry and immunohistochemical analyses of Col1a2-GFP mice at different developmental stages to analyze the characteristics of the lineage$^-$ GFP$^+$ population. GFP$^+$ cells were present in alveolar walls as well as in peribronchiolar and perivascular regions in Col1a2-GFP mice (Tsukui et al., 2013) at the examined time points and were negative for CD31, CD45, Epcam, or Ter119 (Figures S1A and S1B). Peribronchiolar and perivascular GFP$^+$ cells were co-labeled with α-SMA$^+$ smooth muscle cells (Figure S1B) (De Val et al., 2002). Since we depleted CD146$^+$ smooth muscle cells before cell sorting, the analyzed GFP$^+$ CD146$^-$ population comprised alveolar fibroblasts, including Pdgfra$^+$ and Pdgfra$^-$ cells (Figures S1C and S1D). No distinct GFP$^+$ Pdgfrb$^+$ CD146$^-$ mesenchymal population was isolated by flow cytometry (Figure S1C). Transcriptome data for E13.5, E15.5, P14, and P56 epithelial cells of C57BL/6J mice were also included in the analysis.

We first analyzed the transcriptome of epithelial cells (Figure 1C) and fibroblasts (Figure 1D) to evaluate transcriptional changes during alveologenesis and in mature lungs. In epithelial cells, the expression of AEC2 marker genes (Treutlein et al., 2014), such as *Sftpa1*, *Sftpb*, and *Sftpc*, as well as club and ciliated cell marker genes (Treutlein et al., 2014) increased in a time-dependent manner (Figure 1C). In contrast, the expression of genes known to be associated with early lung development, such as *Sox9* and *Foxp2* (Hogan et al., 2014), decreased over time (Figure 1C). The levels of AEC1 marker genes (Treutlein et al., 2014) peaked at E18.5–P0.5 before gradually decreasing (Figure 1C). A qPCR analysis revealed trends in the expression of AEC1/AEC2 markers that were similar to those observed by SAGE-seq analysis (Figures S2A and S2B). Hierarchical clustering of epithelial cells based on their transcriptome revealed that E13.5 and E15.5 epithelial cells clustered separately from other epithelial cells (Figure 1E). These results suggest that the transcriptome data reflected the development and maturation of epithelial cells.

The expression levels of the fibroblast marker genes *Eln*, *Vim*, *Acta2*, and *Col1a2* (Tsukui et al., 2013) as well as *Plin2*, which encodes a protein that delivers lipids within the fibroblast cytosol to adjacent AEC2 (Schultz et al., 2002), were elevated throughout lung development but were especially high in the perinatal period or saccular stage (E17.5–P5) (Figure 1D). Retinoic acid signaling-associated transcription factors *Rara* and *Rarg* (McGowan et al., 1995) were highly expressed at this stage (E18.5–P2) (Figure 1D). Wnt receptors *Lrp5* and *Lrp6* were highly expressed in the mature state, but *Tcf7l1*, a downstream gene of Wnt signaling (Shy et al., 2013), was gradually downregulated as the lungs matured (Figure 1D). Fibroblast growth factor (Fgf) ligands and receptor (*Fgfr1*) were highly expressed in the mature lungs (Figure 1D); this corresponded with epithelial expression of *Fgfr2* (Figure 1C), suggesting an important role for Fgf signaling at this stage. Interestingly, Sonic hedgehog (Shh) signaling-associated genes were specifically upregulated in P2 (Figure 1D), which coincided with epithelial upregulation of *Shh* at P2 (Figure 1C) (Peng et al., 2015). Hierarchical clustering of fibroblasts based on their transcriptome showed that P28 (the end of alveologenesis) and P56 (mature state) clustered separately from the other developmental stages (Figure 1F).

We next identified differentially expressed genes (DEGs; genes with adjusted $p < 0.05$, maximum expression >50) in the transcriptome data of epithelial cells (3,382 genes) and fibroblasts (3,437 genes). Using the CLICK method (Sharan et al., 2003), we identified 13 distinct clusters of DEGs (C1–C13; Figure 2A and Table S1) for epithelial cells and 12 for fibroblasts (C1–C12; Figure 2B and Table S1). Importantly, the levels of genes in epithelial cluster C1 increased with lung maturation and peaked at P28. Gene Ontology (GO) enrichment analysis (Ashburner et al., 2000) and Kyoto Encyclopedia of Genes and Genomes (KEGG) pathway enrichment analysis (Kanehisa et al., 2017) of epithelial C1 revealed that genes associated with lipid/fatty acid metabolism, epithelium development, and the mitogen-activated protein kinase (MAPK) cascade were highly enriched (Figure 2C and Table S2). Epithelial C1 genes annotated to the MAPK cascade (Table S2) included downstream factors (*Mapk3*) (Plotnikov et al., 2011) as well as those associated with Wnt signaling (*Gsk3b* and *APC*) (Volckaert and De Langhe, 2015) and Fgf signaling (*Fgfr2*) (Volckaert and De Langhe, 2015), suggesting important roles for Wnt/Fgf signaling in alveologenesis. In contrast, genes included in epithelial cluster C3 were highly expressed at E18.5–P2 (saccular stage) and included angiogenesis-associated genes, such as *Vegfa* and *Pdgfa* (Figure 2A and Table S2) (Chao et al., 2016). This suggests that genes regulating angiogenesis rather than epithelium maturation play important roles at the saccular as compared with the alveolar maturation stage (P5–P28). Genes included in epithelial clusters C2 and C4 were highly expressed at E13.5–E18.5 and included genes associated with cell division, which could reflect the high proliferative potential of epithelial cells during this period.

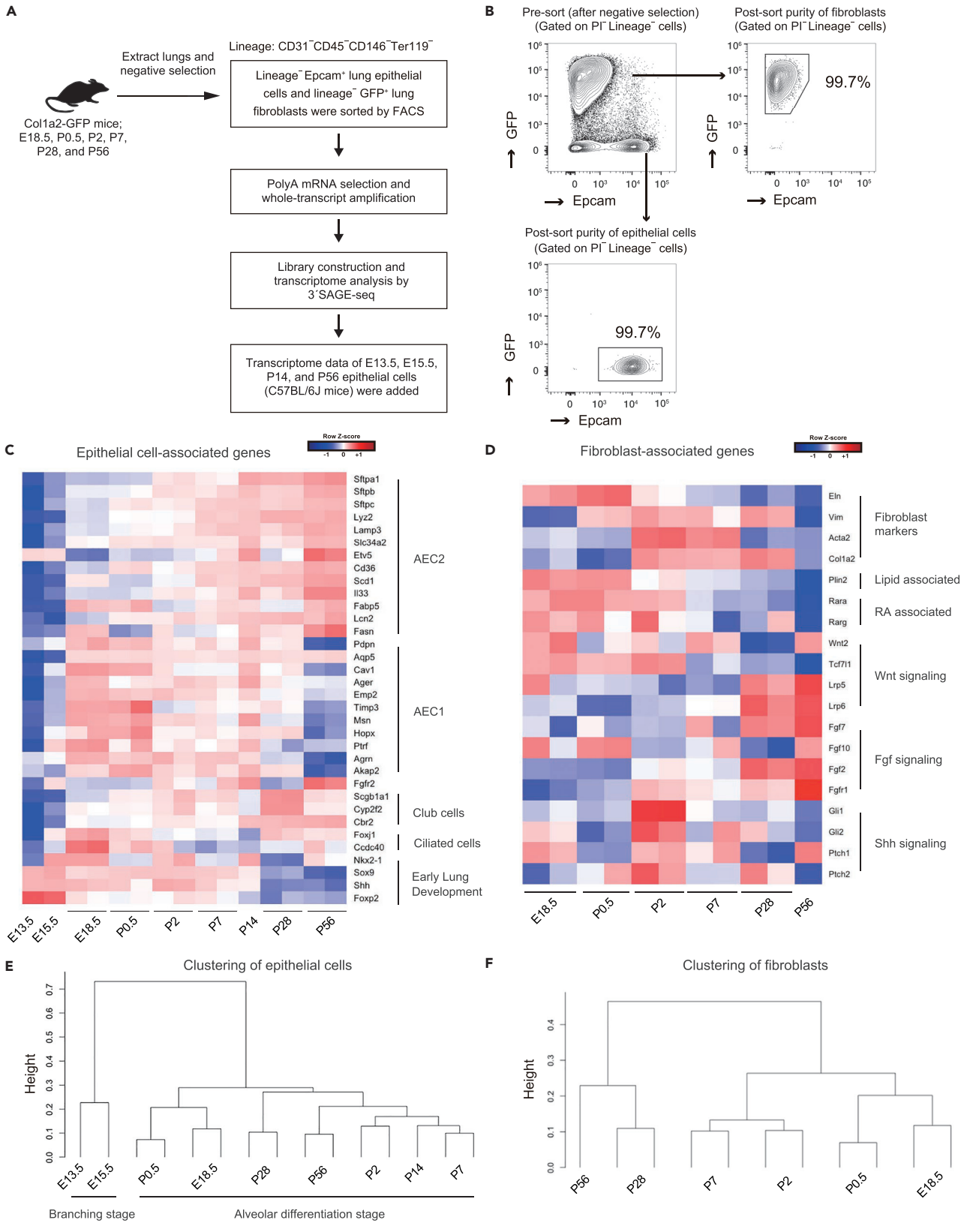
A
Extract lungs and negative selection
Lineage: CD31⁻CD45⁻CD146⁻Ter119⁻
Col1a2-GFP mice; E18.5, P0.5, P2, P7, P28, and P56
Lineage⁻Epcam⁺ lung epithelial cells and lineage⁻ GFP⁺ lung fibroblasts were sorted by FACS
PolyA mRNA selection and whole-transcript amplification
Library construction and transcriptome analysis by 3′SAGE-seq
Transcriptome data of E13.5, E15.5, P14, and P56 epithelial cells (C57BL/6J mice) were added
B
Pre-sort (after negative selection) (Gated on PI⁻ Lineage⁻ cells)
Post-sort purity of fibroblasts (Gated on PI⁻ Lineage⁻ cells)
99.7%
Post-sort purity of epithelial cells (Gated on PI⁻ Lineage⁻ cells)
99.7%
GFP
Epcam
C
Epithelial cell-associated genes
Row Z-score
Sftpa1
Sftpb
Sftpc
Lyz2
Lamp3
Slc34a2
Etv5
Cd36
Scd1
Il33
Fabp5
Lcn2
Fasn
Pdpn
Aqp5
Cav1
Ager
Emp2
Timp3
Msn
Hopx
Ptrf
Agrn
Akap2
Fgfr2
Scgb1a1
Cyp2f2
Cbr2
Foxj1
Ccdc40
Nkx2-1
Sox9
Shh
Foxp2
AEC2
AEC1
Club cells
Ciliated cells
Early Lung Development
E13.5
E15.5
E18.5
P0.5
P2
P7
P14
P28
P56
D
Fibroblast-associated genes
Row Z-score
Eln
Vim
Acta2
Col1a2
Plin2
Rara
Rarg
Wnt2
Tcf7l1
Lrp5
Lrp6
Fgf7
Fgf10
Fgf2
Fgfr1
Gli1
Gli2
Ptch1
Ptch2
Fibroblast markers
Lipid associated
RA associated
Wnt signaling
Fgf signaling
Shh signaling
E18.5
P0.5
P2
P7
P28
P56
E
Clustering of epithelial cells
Height
E13.5
E15.5
P0.5
E18.5
P28
P56
P2
P14
P7
Branching stage
Alveolar differentiation stage
F
Clustering of fibroblasts
Height
P56
P28
P7
P2
P0.5
E18.5

Figure 1. Time Series Global Transcriptome Analysis of Epithelial Cells and Fibroblasts during Alveologenesis

(A) Experimental scheme of transcriptomic analysis of E18.5, P0.5, P2, P7, P28, and P56 lung epithelial cells and fibroblasts (n = 2 animals except for P56 fibroblasts [n = 1]). FACS, fluorescence-activated cell sorting.

(B) Gating scheme for lung epithelial cells and fibroblasts and purity of cells after cell sorting. Representative plots of P56 mice are shown.

(C) Heatmap of selected AEC2, AEC1, and club cell markers and early lung development-associated genes.

(D) Heatmap of selected fibroblast markers and genes associated with lipids; retinoic acids; and Wnt, Fgf, and Shh signaling.

(E and F) Hierarchical clustering by dendrogram of epithelial cells (E) and fibroblasts (F) based on their transcriptome.

See also Figures S1 and S2, and Tables S7 and S8.

The expression levels of genes in fibroblast clusters C2 and C3 tended to increase with lung maturation, peaking at P56 and P28, respectively (Figure 2B). These clusters included genes associated with the MAPK cascade and Wnt and Hippo signaling (Figure 2D and Table S2). Fibroblast C2 genes annotated to the MAPK cascade (Table S2) included *Gsk3b*, *Fgf2*, *Fgfr1*, *Fgfr3*, *Tgfb3*, and *Tgfbr3*, suggesting that Wnt, Fgf, and Tgf-β signaling pathways are activated in fibroblasts. Fibroblast C2 genes were associated with Wnt signaling (Table S2) and included *Lrp5* and *Lrp6* (Volckaert and De Langhe, 2015). These results suggest that Wnt/Fgf/Tgf-β signaling-associated genes were enriched in fibroblasts in alveologenesis and in the mature state. Genes included in fibroblast clusters C1, C4, and C5 were highly expressed at E18.5–P2 and included those associated with cell division, which could reflect the high proliferative potential of fibroblasts during these periods as compared with later stages. Collectively, our transcriptome analysis revealed significant changes in transcriptional profiles throughout lung development and identified several signaling pathways that may regulate alveologenesis and AEC2 maintenance.

Signaling Pathways Activated during Alveologenesis and in Mature Lungs

To identify lung fibroblast-epithelial interactions that potentially regulate alveologenesis and homeostasis of the alveolar stem cell niche, we examined genes expressed in fibroblasts and epithelial cells encoding extracellular molecules and cell surface receptor molecules, respectively (Figure 3A). We then reconstructed fibroblast-epithelial interactions according to interaction information provided by the KEGG database (Figures 3A and 3B; Table S3). We also identified genes expressed in fibroblasts and epithelial cells encoding cell surface receptors and extracellular molecules, respectively, and reconstructed epithelial-fibroblast (Table S4), fibroblast-fibroblast (Table S5), and epithelial-epithelial interactions (Table S6). To investigate whether the fibroblast-epithelial interactions were applicable to those between fibroblasts and AEC2, we used publicly available transcriptome data of lung mesenchymal subpopulations (Zepp et al., 2017) and analyzed the expression of fibroblast-expressed ligands in mesenchymal subpopulations supporting AEC2. We found that most fibroblast-expressed ligands were highly expressed in lung Axin2$^+$ Pdgfra$^+$ or Pdgfra$^+$ mesenchymal cells (Figure 3C), which support AEC2 and generate alveolospheres.

The above-mentioned results suggested that the identified interactions were associated with fibroblast-AEC2 interactions. Moreover, the expression levels of these fibroblast ligands tended to be high during alveolar maturation (P5–P28) and in the mature lung stage (P56) as compared with the saccular stage (E17.5–P2) (Figure 3D), suggesting that the interactions were associated with AEC2 proliferation and differentiation in the former and not the latter periods. Specifically, fibroblast ligands *Fgf2*, *Fgf7* (Figure 3E), *Bmp4*, *Bmp5* (Figure 3G), *Tgfb1*, and *Tgfb3* (Figure 3I) as well as epithelial *Fgfr2* (Figure 3F) and *Bmpr2* (Figure 3H) were upregulated as the lungs matured, suggesting specific roles for Fgf, Bmp, and Tgf-β signaling in alveologenesis and lung maturation. Fibroblast *Fgf10* expression was high throughout the development (Figure 3E), but considering the high expression level of its receptor *Fgfr2* during alveolar maturation and in the mature lung stage, its specific role in alveologenesis was also presumed. Although the levels of direct Notch ligands were low in fibroblasts (data not shown), the corresponding receptor *Notch2* was highly expressed in epithelial cells in the alveologenesis stage (Figure 3K), suggesting that Notch signaling is involved in alveologenesis (Tsao et al., 2016). *Wnt2* and *Wnt5a* (Figure 3L) levels in fibroblasts as well as epithelial *Lrp5* (Figure 3M) and *Tgfbr1* (Figure 3J) remained relatively constant throughout lung development. Given the high overall expression level of *Lrp5*, we presumed that Wnt signaling plays a role in alveologenesis. We also performed a statistical assessment of linear relationships between CLICK-identified fibroblast clusters and epithelial cell clusters (Figure S3A) as well as fibroblast ligands and epithelial receptors (Figure S3B) and found that fibroblast cluster 2 (including *Fgf7* and *Fgf2*) and epithelial cluster 1 (including *Fgfr2*) were positively correlated ($r = 0.49$, $p = 0.1$). Although they were non-significant, we found positive correlations between *Fgf7*/*Fgfr2* ($r = 0.22$, $p = 0.5$), *Fgf10*/*Fgfr2* ($r = 0.31$, $p = 0.3$), *Bmp5*/*Bmpr2* ($r = 0.16$, $p = 0.6$), *Tgfb1*/*Tgfbr1* ($r = 0.4$, $p = 0.2$), and *Tgfb3*/*Tgfbr1* ($r = 0.41$, $p = 0.2$) (Figure S3B).

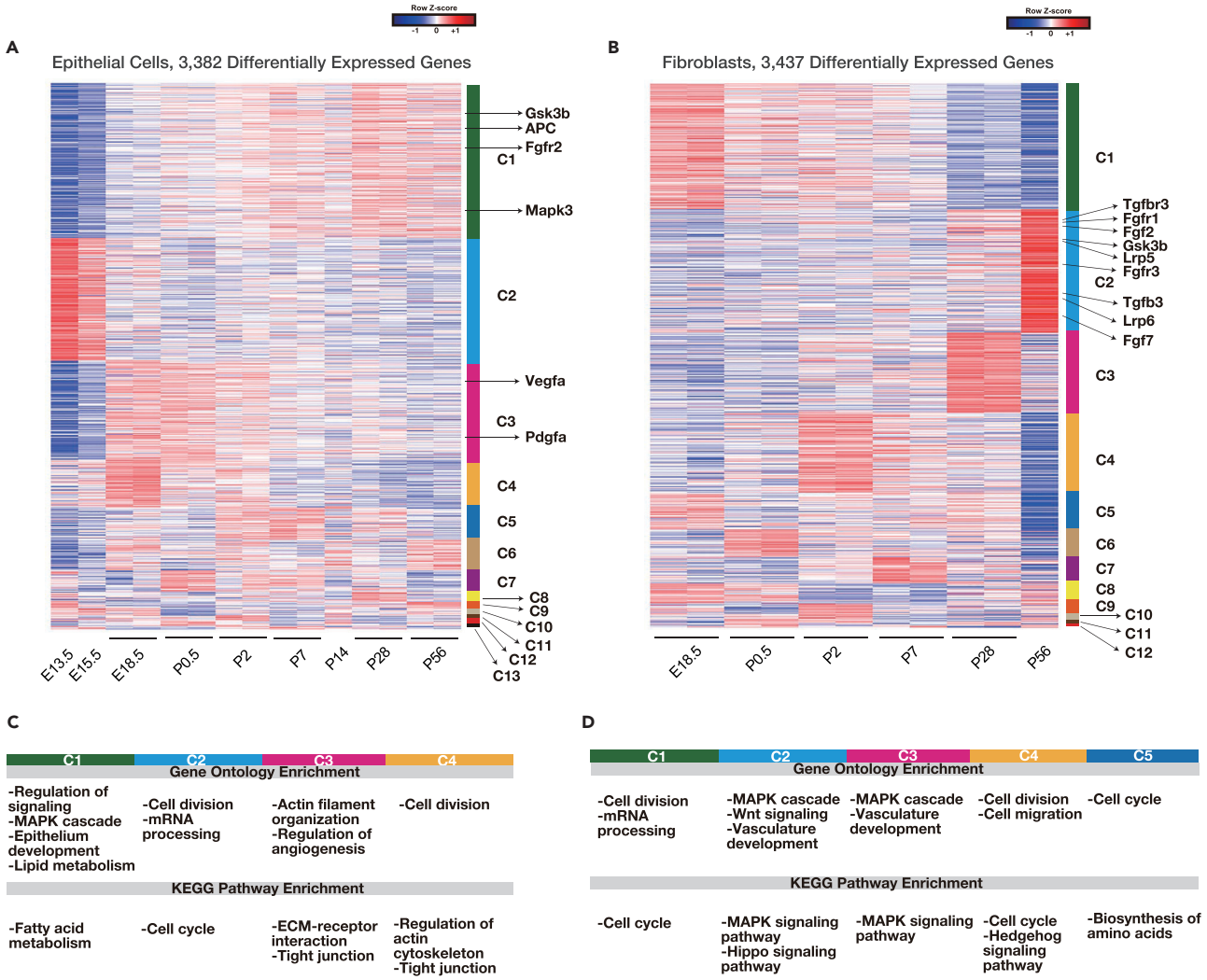

Figure 2. Distinct DEG Clusters at Different Developmental Stages

(A and B) Heatmap of 3,382 DEGs in epithelial cells (A) and 3,437 DEGs in fibroblasts (B) after clustering. Cluster numbers are shown on the right. (C and D) GO and KEGG pathway enrichment analyses for each epithelial (C) and fibroblast (D) cluster (Table S2).

See also Figure S3.

Thus, the results of the interactome analysis suggest that interactions between fibroblasts and AEC2 in alveologenesis and in mature lungs involve Fgf, Bmp, Tgf-β, Notch, and Wnt signaling.

Fibroblast Ligands and Signaling Pathway Inhibitors Promote Alveolosphere Growth In Vitro

To assess the significance of fibroblast-AEC2 interactions *in vitro*, we performed an alveolosphere formation assay by directly co-culturing lineage (CD31, CD45, CD146 and Ter119)$^-$ Epcam$^+$ EGFP$^+$ epithelial cells from CAG-EGFP mice and fibroblasts from C57BL/6J mice (Figure 4A) (Barkauskas et al., 2013). Epcam$^+$ epithelial cells included AEC2 (89.14% ± 1.34%), club cells (6.85% ± 0.46%), ciliated cells (5.19% ± 0.90%), and AEC1 (0.83% ± 0.49%) (Figure 4C). After alveolosphere generation, EGFP$^+$ epithelial cells and EGFP$^-$ fibroblasts were sorted for qPCR analysis. As a control experiment, epithelial cells and fibroblasts were indirectly co-cultured (Figure 4B), but this resulted in no epithelial cell proliferation (data not shown), suggesting that factors expressed higher in direct co-cultures than in indirect co-cultures may promote alveolosphere formation. To understand the mechanism, fibroblasts obtained from the indirect culture were lysed and analyzed by qPCR. Although bulk epithelial cells were sorted for co-culture, the direct culture assay generated mostly Hopx$^+$ Sftpc$^+$ alveolospheres, as determined by

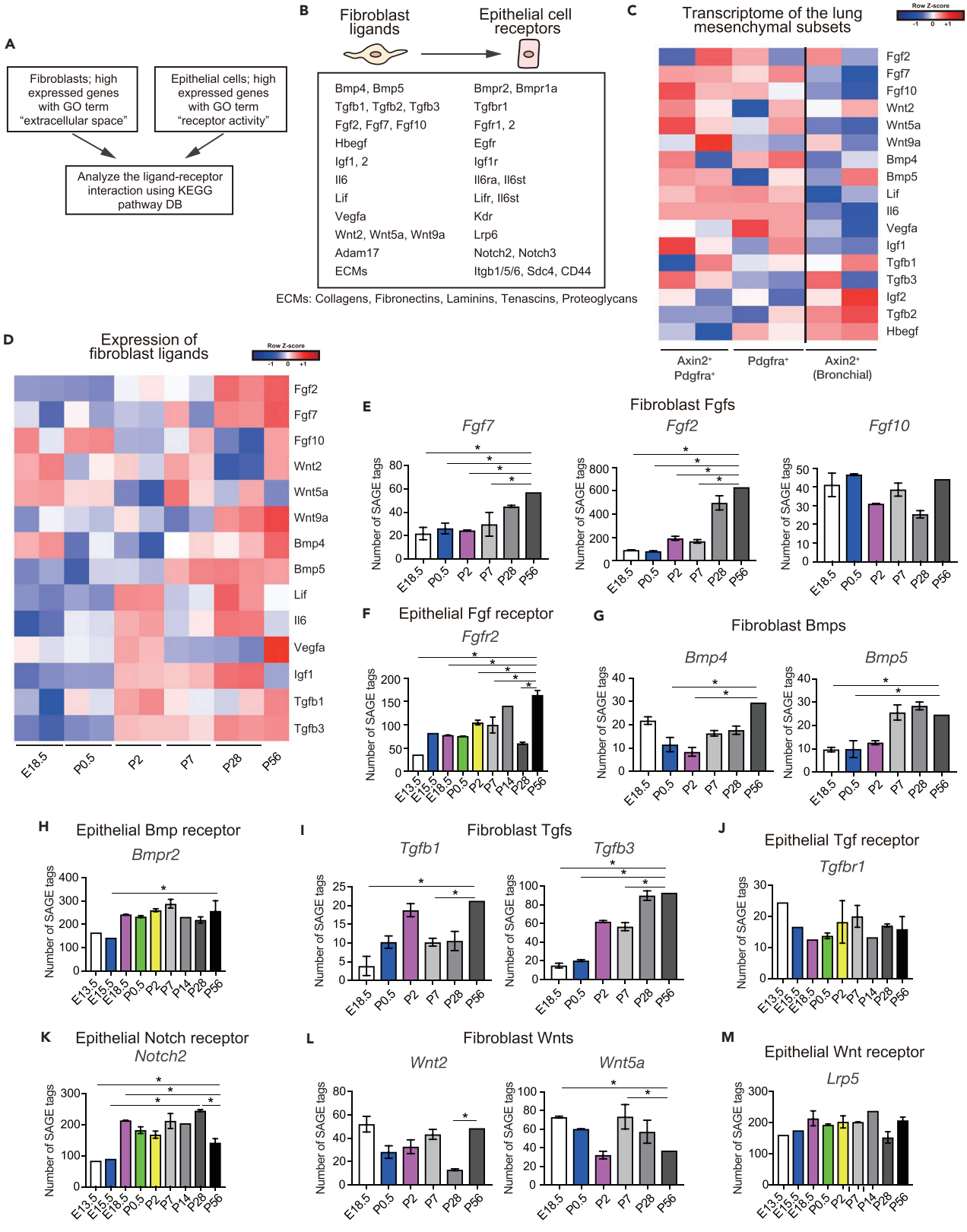
A
Fibroblasts; high expressed genes with GO term "extracellular space"
Epithelial cells; high expressed genes with GO term "receptor activity"
Analyze the ligand-receptor interaction using KEGG pathway DB
B
Fibroblast ligands
Epithelial cell receptors
Bmp4, Bmp5 | Bmpr2, Bmpr1a
Tgfb1, Tgfb2, Tgfb3 | Tgfbr1
Fgf2, Fgf7, Fgf10 | Fgfr1, 2
Hbegf | Egfr
Igf1, 2 | Igf1r
Il6 | Il6ra, Il6st
Lif | Lifr, Il6st
Vegfa | Kdr
Wnt2, Wnt5a, Wnt9a | Lrp6
Adam17 | Notch2, Notch3
ECMs | Itgb1/5/6, Sdc4, CD44
ECMs: Collagens, Fibronectins, Laminins, Tenascins, Proteoglycans
C
Transcriptome of the lung mesenchymal subsets
Row Z-score
Fgf2
Fgf7
Fgf10
Wnt2
Wnt5a
Wnt9a
Bmp4
Bmp5
Lif
Il6
Vegfa
Igf1
Tgfb1
Tgfb3
Igf2
Tgfb2
Hbegf
Axin2+ Pdgfra+
Pdgfra+
Axin2+ (Bronchial)
D
Expression of fibroblast ligands
E18.5
P0.5
P2
P7
P28
P56
E
Fibroblast Fgfs
Fgf7
Fgf2
Fgf10
Number of SAGE tags
F
Epithelial Fgf receptor
Fgfr2
G
Fibroblast Bmps
Bmp4
Bmp5
H
Epithelial Bmp receptor
Bmpr2
E13.5
E15.5
P14
I
Fibroblast Tgfs
Tgfb1
Tgfb3
J
Epithelial Tgf receptor
Tgfbr1
K
Epithelial Notch receptor
Notch2
L
Fibroblast Wnts
Wnt2
Wnt5a
M
Epithelial Wnt receptor
Lrp5

Figure 3. Signaling Pathways Upregulated during Alveologenesis and in Mature Lungs

(A and B) Schematic for (A) and summary of (B) fibroblast-epithelial interactome analysis (Table S3). *Adam17* is not a direct ligand to *Notch2* or *Notch3* but was detected in the analysis.

(C and D) Heatmap of fibroblast ligand-encoding genes based on transcriptome data of lung mesenchymal subsets (GSE92699) (C) and our time course transcriptome data (D).

(E–M) Number of SAGE tags (expression after standardization) of the selected genes. Data represent mean ± SEM. *Adjusted $p < 0.05$; normalized data were examined for statistical significance using TCC package (Sun et al., 2013).

See also Figure S3.

immunohistochemistry (Figures 4D–4F) and qPCR (Figures 4G–4I). All 56 immunostained spheres (randomly selected serial sections of 56 spheres fixed after 14 days in culture from three independent experiments) were positive for Sftpc and one Sftpc$^+$ sphere included Sftpc$^-$ Scgb1a1$^+$ cells (data not shown) (Lee et al., 2017). We did not detect acetylated tubulin$^+$ ciliated cells or Krt5$^+$ basal cells (Figure 4F). The expression of marker genes of AEC1 (*Aqp5* and *Hopx*; Figure 4G) and AEC2 (*Sftpc* and *Sftpd*; Figure 4H) in epithelial cells obtained from the alveolospheres, but not non-alveolar epithelial cell marker genes (*Foxj1* and *Scgb1a1*; Figure 4I), was confirmed by qPCR.

The qPCR analysis revealed upregulation of *Fgf7* and *Fgf10* in directly but not indirectly co-cultured fibroblasts (Figure 5A). Moreover, upregulation of *Fgfr2b*, a specific receptor for *Fgf7* and *Fgf10* (Ornitz and Itoh, 2015), was observed in co-cultured epithelial cells (Figure 5A), suggesting that fibroblasts might upregulate Fgf7 and Fgf10 to interact with AEC2. Given that adding mouse (m)Fgf7 (Zepp et al., 2017) and human (h) Fgf10 (Zacharias et al., 2018) to direct co-cultures increased alveolosphere size and increased colony-forming efficiency, respectively (Figures 5B, 5I, and S4E), it was presumed that Fgf7 and Fgf10 are associated with AEC2 growth. *Fgf2* was expressed in fibroblasts and mFgf2 promoted alveolosphere growth (Figures 5I, S4A, S4B, and S4E), but *Fgfr1c* was expressed only in fibroblasts (Figure S4A), suggesting that Fgf2 is secreted by fibroblasts for self-maintenance. *Wnt2* and *Wnt5a* were upregulated in directly co-cultured fibroblasts (Figure 5C), whereas *Tcf7l1*, a gene downstream of Wnt signaling (Shy et al., 2013), was upregulated in both co-cultured fibroblasts and epithelial cells (Figure 5C). Since several Wnts can be expressed in lung AEC2 (Nabhan et al., 2018), it was presumed that different Wnts are expressed in and mediate the interaction between fibroblasts and AEC2. The GSK-3β inhibitor CHIR99021, a canonical Wnt pathway agonist (Frank et al., 2016), increased alveolosphere size and decreased colony-forming efficiency (Figures 5D, 5I, and S4E). These findings suggest that Wnt signaling is involved in fibroblast-AEC2 interactions. Regarding Tgf-β/Bmp signaling, *Tgfb1*, *Bmp4*, and *Bmp5* were more highly expressed in directly as compared with indirectly co-cultured fibroblasts, and their receptors *Tgfbr2*, *Bmpr1a*, and *Bmpr2* were expressed in both fibroblasts and AEC2 (Figures 5E, 5G, and S4C). Mouse (m)Bmp4 (Zepp et al., 2017) and mBmp5 decreased alveolosphere size (Figures 5H, 5I, S4D, and S4E; no significant change in colony-forming efficiency), and human TGF-β1 interrupted sphere formation (Figures 5F, 5I, and S4E). On the other hand, the TGF-β inhibitor SB431542 (Jain et al., 2015) and Bmp4 inhibitor mNoggin increased alveolosphere size (Figures 5F, 5H, 5I, and S4E; no significant change in colony-forming efficiency), indicating that Bmp/Tgf-β signaling might inhibit AEC2 in the context of fibroblast-epithelial interactions. To assess the number of proliferating cells within the co-culture assays, we used epithelial cells obtained from Fucci mice (Sakaue-Sawano et al., 2008; Tomura et al., 2013) and assessed Fucci-green (mAG)-positive epithelial cells in the wells by flow cytometry (Figures S4F and S4G) and found that the number of actively proliferating (mAG positive) epithelial cells was increased upon addition of SB431542, Fgf7, and Fgf2 (Figures S4F and S4G). These results demonstrate that Fgf7/10, Wnt (Figure 5J), and Bmp/Tgf-β signaling mediate AEC2-fibroblasts interactions and are important regulators of AEC2.

Specific Factors Are Required to Induce Fibroblast-Free Alveolospheres

The results of the co-culture assay suggested that several signaling pathways are critical for AEC2 proliferation. We hypothesized that alveolospheres could be induced to form by adding several fibroblast-derived ligands and signaling inhibitors. To investigate whether fibroblast-free alveolosphere formation was possible, adult epithelial cells from CAG-EGFP mice were sorted and cultured in Matrigel with various combinations of fibroblast-derived ligands and signaling inhibitors. We found that mFgf7, mNoggin, SB431542, CHIR99021, and the Notch ligand Jagged1 (Sato et al., 2009) were necessary to induce the formation of fibroblast-free alveolospheres (Figures 6A–6D and S5A). Jagged1 was added because inactivation of Jagged1 was reported to cause defects in alveologenesis in the developing distal lung (Zhang et al., 2013) and because *Notch2* was highly expressed in the adult epithelium (Figure 3K). Single-molecule treatment with mFgf7, mNoggin, SB431542, or CHIR99021 did not induce sphere generation, and their removal from the

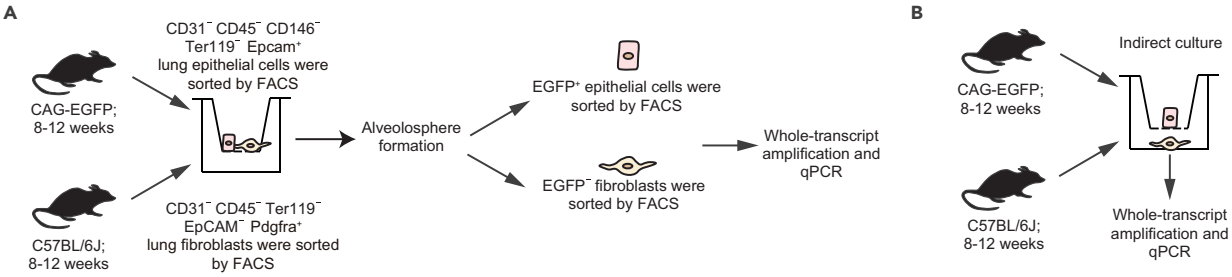
A
CAG-EGFP;
8-12 weeks
CD31⁻ CD45⁻ CD146⁻
Ter119⁻ Epcam⁺
lung epithelial cells were
sorted by FACS
C57BL/6J;
8-12 weeks
CD31⁻ CD45⁻ Ter119⁻
EpCAM⁻ Pdgfra⁺
lung fibroblasts were sorted
by FACS
Alveolosphere
formation
EGFP⁺ epithelial cells were
sorted by FACS
EGFP⁻ fibroblasts were
sorted by FACS
Whole-transcript
amplification and
qPCR
B
CAG-EGFP;
8-12 weeks
C57BL/6J;
8-12 weeks
Indirect culture
Whole-transcript
amplification and
qPCR

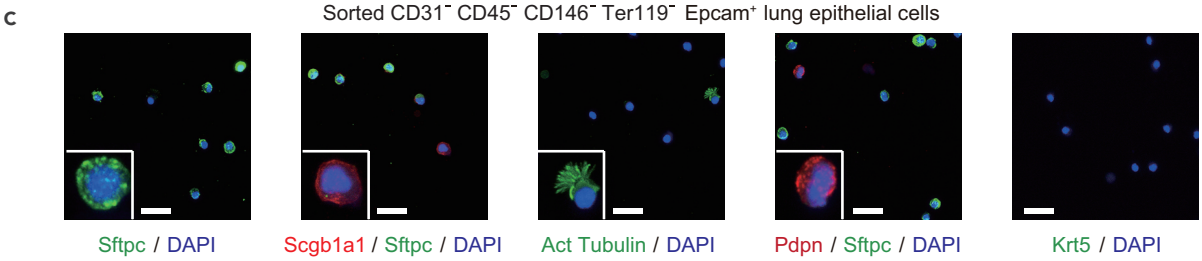
C
Sorted CD31⁻ CD45⁻ CD146⁻ Ter119⁻ Epcam⁺ lung epithelial cells
Sftpc / DAPI
Scgb1a1 / Sftpc / DAPI
Act Tubulin / DAPI
Pdpn / Sftpc / DAPI
Krt5 / DAPI

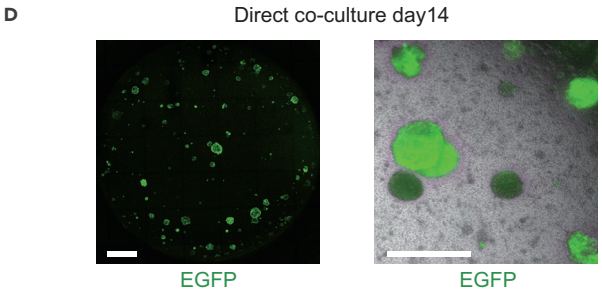
D
Direct co-culture day14
EGFP
EGFP

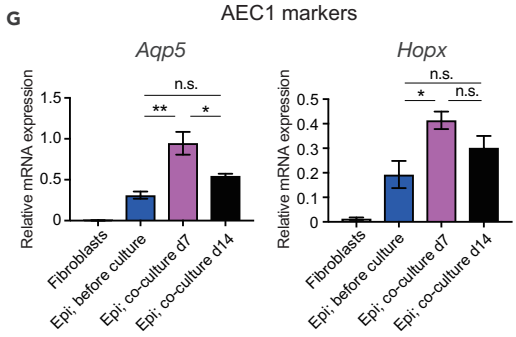
G
AEC1 markers
Aqp5
Hopx
Relative mRNA expression
n.s.
**
*
Fibroblasts
Epi; before culture
Epi; co-culture d7
Epi; co-culture d14

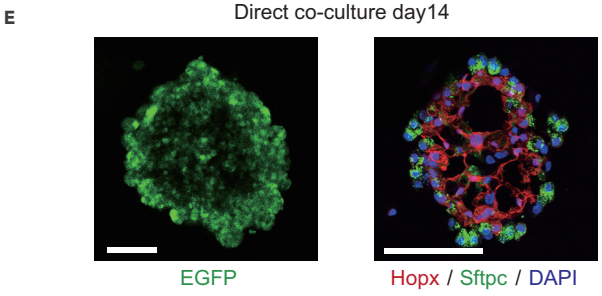
E
Direct co-culture day14
EGFP
Hopx / Sftpc / DAPI

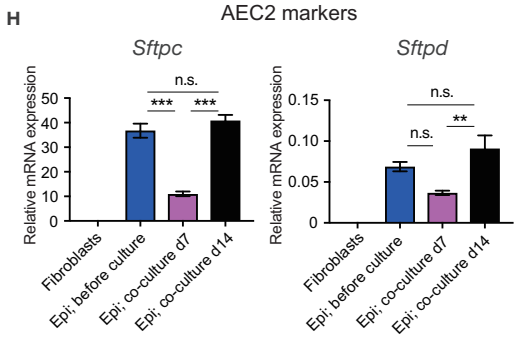
H
AEC2 markers
Sftpc
Sftpd
Relative mRNA expression
n.s.
***
**
Fibroblasts
Epi; before culture
Epi; co-culture d7
Epi; co-culture d14

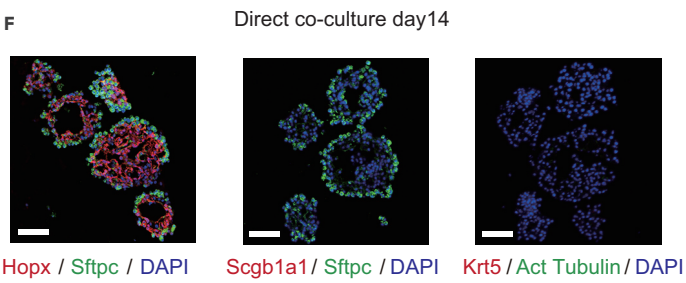
F
Direct co-culture day14
Hopx / Sftpc / DAPI
Scgb1a1 / Sftpc / DAPI
Krt5 / Act Tubulin / DAPI

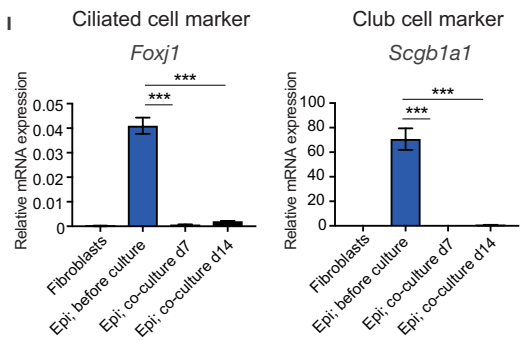
I
Ciliated cell marker
Club cell marker
Foxj1
Scgb1a1
Relative mRNA expression
***
Fibroblasts
Epi; before culture
Epi; co-culture d7
Epi; co-culture d14

Figure 4. Alveolospheres Generated from Direct Epithelial-Fibroblast Co-culture

(A) Experimental scheme of alveolosphere formation assay by direct co-culture of 8- to 12-week-old CAG-EGFP epithelial cells and 8- to 12-week-old C57BL/6J fibroblasts.

(B) Experimental scheme of indirect co-culture of epithelial cells and fibroblasts.

(C) Immunocytochemical analysis of sorted Epcam$^+$ cells showing Sftpc$^+$ AEC2, Scgb1a1$^+$ club cells, acetylated tubulin$^+$ ciliated cells, and Pdpn$^+$ AEC1.

(D) Image of a representative well (left; entire Transwell stored in 24-well plates is shown) from direct epithelial-fibroblast co-culture obtained by confocal microscopy and representative merged view obtained by fluorescence microscopy (right).

(E) Enlarged image of the alveolosphere in Figure 4D (left) and alveolosphere labeled with antibodies (right) against Hopx (red) and Sftpc (green).

(F) Collected alveolospheres labeled with antibodies against Hopx/Sftpc (left), Scgb1a1/Sftpc (middle), and Krt5/acetylated tubulin (right).

(G–I) qPCR of AEC1 (G), AEC2 (H), and non-alveolar epithelial (I) markers using cells obtained from direct epithelial-fibroblast co-culture assays (before culture and on days 7 and 14). mRNA levels were normalized to that of *Actb*. Data represent mean ± SEM (n = 3 wells for cultured cells and n = 3 animals for sorted cells) and are representative of two independent experiments. *$p < 0.05$, **$p < 0.01$, ***$p < 0.001$ (one-way ANOVA with Tukey's *post hoc* test).

Scale bars: 25 μm (C), 1 mm (D), and 100 μm (E and F).

combination of molecules resulted in no or weak sphere formation (one sphere formed in 2/6 wells in the absence of SB431542 and one sphere formed in 3/6 wells in the absence of mNoggin; Figure S5A). Although a crucial role of Fgf10 was presumed from co-culture assays, substituting mFgf7 with hFgf10 did not yield spheres (Figure S5A). Omitting Jagged1 from the combination of molecules yielded some spheres (up to four spheres per well), but these were fewer in number (spheres in 8/9 wells, with only one sphere in 4/8 wells) than in Jagged1 supplemented cultures (spheres in 9/9 wells, with 5.9 ± 1.1 spheres per well). The observation that the γ-secretase inhibitor DAPT inhibited sphere formation suggests that Notch signaling has positive effects on alveolosphere formation.

On day 8 of culture, fibroblast-free alveolospheres became larger than day 14 co-cultured alveolospheres (Figure S5B) and were globular with an empty inner part (Figure 6B). Around day 12, the inner part began to fill with cells in a lattice pattern (Figures 6C and 6D). Immunohistochemical analysis revealed that on day 8, the spheres contained Aqp5$^+$ Sftpc$^+$ cells (Figure 6E). We did not detect any Scgb1a1$^+$, acetylated tubulin$^+$, or Krt5$^+$ cells (Figure 6F). On day 14, Aqp5$^+$ AEC1 accumulated inside the spheres (Figure 6G), and qPCR analysis confirmed the expression of AEC1 (Figure 6H) and AEC2 (Figure 6I) markers but not non-alveolar epithelial markers (Figure 6J). In addition, the alveolospheres did not express fibroblast or fibroblast activation marker genes (Tsukui et al., 2013) (Figures S5C and S5D), suggesting an absence of epithelial-mesenchymal transition or fibroblast contamination. Since airway cells were included in the Epcam$^+$ cell population that we used for fibroblast-free culture (Figures 4C and 6A), we sorted the (CD31/CD45/Pdgfra/CD146/Ter119)$^-$ (lineage-negative) CD24$^-$ (airway cell-negative) (Chen et al., 2012) CD34$^-$/Sca1$^-$ (Scgb1a1$^+$/Sftpc$^+$ cell-negative) (Kim et al., 2005) MHCII$^+$/Epcam$^+$ (Hasegawa et al., 2017) population that was enriched in AEC2 (98.45% ± 0.65%; Figures S6A–S6C) and confirmed that it generates alveolospheres under fibroblast-free conditions (Figures S6D–S6G).

The alveolospheres could be passaged even as single-cell suspensions (Figures 7A–7C). Although the colony-forming efficiency of passaged fibroblast-free alveolospheres was less than that of co-cultured alveolospheres, the efficiency of passaged fibroblast-free alveolospheres was stable for at least three passages (P1, 2.57% ± 0.26%; P2, 2.31% ± 0.13%; and P3, 2.24% ± 0.35%) (Figure 7D). We confirmed Sftpc and Aqp5 expression in the passaged alveolospheres and did not detect any non-alveolar markers (Figures 7E and 7F). These results indicate that a specific molecule and inhibitor combination promotes the clonal proliferation of AEC2 and is thus critical for AEC2.

DISCUSSION

To clarify fibroblast-AEC2 cell interactions, we performed a time course SAGE-seq analysis and identified time-specific transcriptional features of epithelial cells and fibroblasts that we used to generate a list of possible fibroblast-AEC2 interactions. We also showed that alveolospheres can be generated under mesenchymal cell-free conditions using a specific set of factors that promote alveolosphere growth in epithelial-fibroblast co-cultures and may thus be critical regulators of AEC2 proliferation.

Our transcriptome analysis revealed stage-specific transcriptional signatures during lung development. E13.5 and E15.5 epithelial cells clustered separately from other epithelial cells by unsupervised hierarchical clustering, which is in accordance with a recent proposal to classify lung development into two distinct processes—branching morphogenesis (E9.5–E16.5) and alveolar epithelial differentiation (E16.5–P30) (Chao et al., 2016). Furthermore, our analysis revealed distinct DEG clusters at each developmental stage,

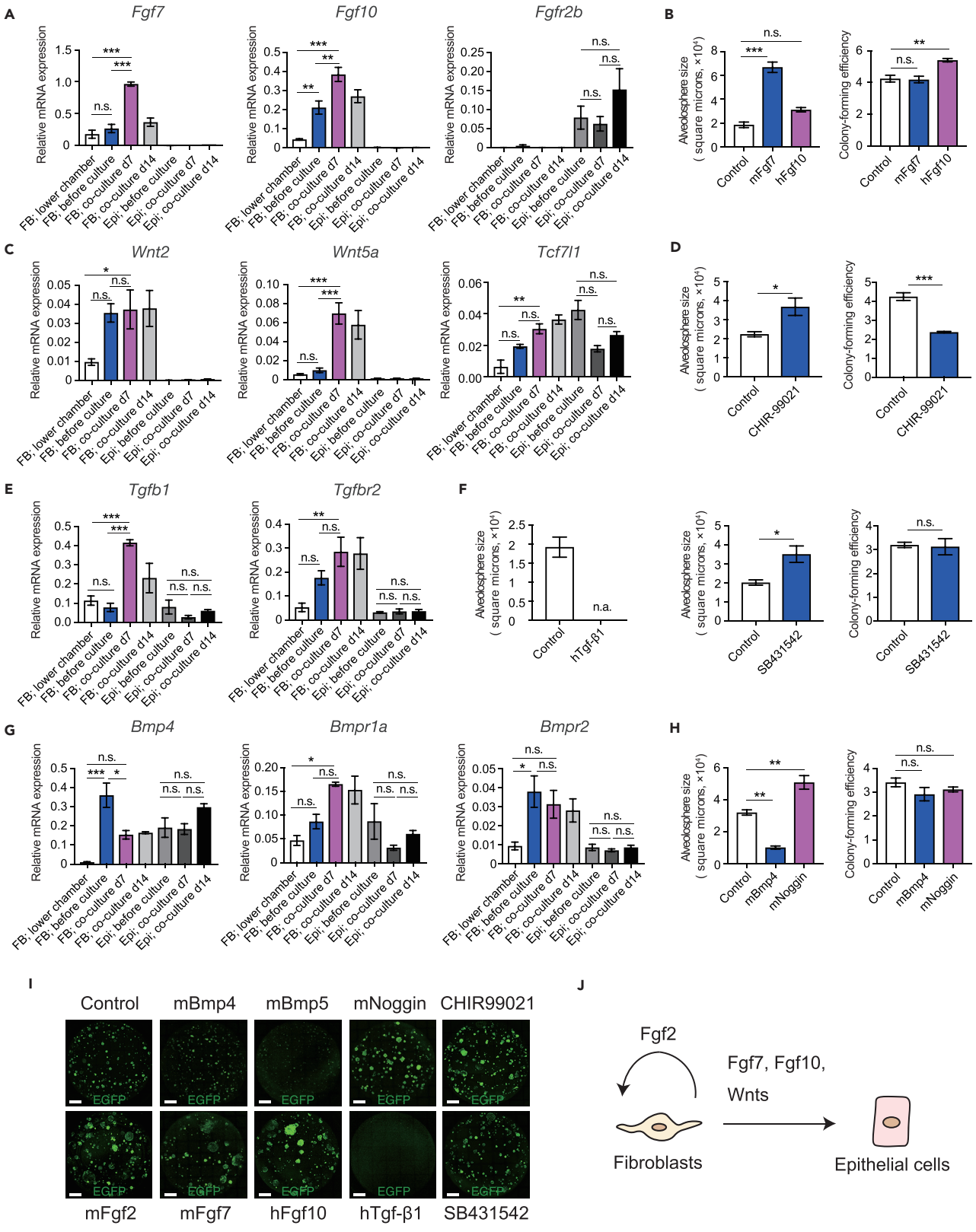
A
Fgf7
Fgf10
Fgfr2b
Relative mRNA expression
FB; lower chamber
FB; before culture
FB; co-culture d7
FB; co-culture d14
Epi; before culture
Epi; co-culture d7
Epi; co-culture d14
B
Alveolosphere size (square microns, ×10⁴)
Colony-forming efficiency
Control
mFgf7
hFgf10
C
Wnt2
Wnt5a
Tcf7l1
D
CHIR-99021
E
Tgfb1
Tgfbr2
F
hTgf-β1
SB431542
G
Bmp4
Bmpr1a
Bmpr2
H
mBmp4
mNoggin
I
Control
mBmp4
mBmp5
mNoggin
CHIR99021
EGFP
mFgf2
mFgf7
hFgf10
hTgf-β1
SB431542
J
Fgf2
Fgf7, Fgf10,
Wnts
Fibroblasts
Epithelial cells

Figure 5. Fibroblast Ligands and Signaling Pathway Inhibitors Promote Alveolosphere Growth *In Vitro*

(A, C, E, and G) qPCR of genes related to Fgf (A), Wnt (C), Tgf-β (E), and Bmp (G) signaling using cells obtained from direct and indirect epithelial-fibroblast co-culture assays before culture and day 7 and 14 (n = 3 wells for cultured cells and n = 3 animals for sorted cells). The data are representative of two independent experiments. For "FB; co-culture d7," data for one sample were not available (n = 2). mRNA levels were normalized to that of *Actb*.

(B, D, F, and H) Alveolosphere size and colony-forming efficiency after adding mFgf7 or hFgf10 (B), CHIR99021 (D), hTGF-β1 or SB431542 (F), and mBmp4 or mNoggin (H). Sphere size was averaged for alveolospheres in each well. To calculate colony-forming efficiency, all colonies formed in each well were counted and the number of colonies was divided by 5×10^3 (epithelial cells plated). Data are shown for n = 3 wells and are representative of two independent experiments.

(I) Representative wells (epithelial cells; EGFP; entire Transwell stored in 24-well plates is shown) on day 14 after adding fibroblast ligand or signaling pathway inhibitor.

(J) Schematic for Fgf and Wnt signaling in fibroblast-epithelial interactions. Arrowheads indicate presumed activating signals.

Data represent mean ± SEM. *p < 0.05, **p < 0.01, ***p < 0.001 (one-way ANOVA with Tukey's *post hoc* test or Student's t test). Scale bar: 1 mm. See also Figure S4.

including the saccular (E17.5–P5) and alveolar maturation (P5–P28) stages, that differed in terms of GO and KEGG pathway enrichment, implying that each process is governed by distinct molecular mechanisms. For example, the Shh signaling pathway was specifically enriched in fibroblast C4 by KEGG pathway enrichment analysis, and the expression of Shh-related genes was accordingly upregulated at P2, suggesting that this pathway is activated at the saccular stage. Our time course transcriptome data provide a resource for future studies on the mechanisms of lung development.

The results of our epithelial-fibroblast co-culture alveolosphere formation assay showed that Fgf/Wnt signaling stimulated, whereas Tgf-β/Bmp signaling suppressed, alveolosphere growth. Fgf signaling has been shown to play a critical role in lung development (Ornitz and Itoh, 2015); AEC2 obtained from Sftpc-CreERT2:R26R-EYFP mice revealed that Fgf7 promoted alveolosphere growth (Zepp et al., 2017), which is in accordance with our findings that this effect was induced by Fgf2 and Fgf10. Fgf2 was expressed in fibroblasts but not in epithelial cells and presumably acted on fibroblasts themselves. Experiments using Fgf2 knockout mice demonstrated that Fgf2 was required for epithelial repair and maintenance of epithelial integrity following bleomycin injury (Guzy et al., 2015). Our data suggest that this may be due to the suppression of fibroblast activation and proliferation required for alveolar damage repair. Although very important, the reasons accounting for why direct contact of epithelial cells with fibroblasts is required for alveolosphere formation and why direct co-culture drives upregulation of fibroblast ligands, such as Fgf7 and Fgf10, are unclear. Because *Tcf7l1* was upregulated in both co-cultured fibroblasts and epithelial cells, it was presumed that different Wnts are expressed in both fibroblasts and epithelial cells and mediate the interaction between fibroblasts and AEC2. Wnts are signals with a typical range of 1–2 cells (Farin et al., 2016), and therefore, the mutual Wnt interactions between epithelial cells and fibroblasts that exist only in direct culture could be one of the reasons why direct co-culture generates alveolospheres and upregulates Fgf7 and Fgf10 in fibroblasts.

Fibroblast-free alveolospheres were generated by adding Tgf-β, Bmp4, and GSK-3β inhibitors and Fgf7 and Notch ligands to the culture medium, indicating that both positive and negative regulation in the form of Fgf/Wnt/Notch and Tgf-β/Bmp signaling, respectively, are required for AEC2 proliferation. Since receptors of both Bmp (*Bmpr1a/2*) and Tgf-β (*Tgfbr1/2*) are expressed in epithelial cells and fibroblasts, the results obtained from the co-culture assay are not applicable to the fibroblast-AEC2 interaction. However, we directly demonstrated with the fibroblast-free alveolosphere formation assay that Tgf-β/Bmp4 inhibition was necessary for AEC2 proliferation. Tgf-β maintains bone marrow hematopoietic stem cells in a state of hibernation (Yamazaki et al., 2011), and we presume that Tgf-β family members also act on AEC2 to maintain their quiescence in tissue homeostasis. However, the potential roles of autocrinological and paracrinological effects of Tgf-β/Bmp signaling in the context of the alveolar stem cell niche *in vivo* remain to be determined. Wnt signaling has been reported to be a critical pathway for AEC2 (Frank et al., 2016; Nabhan et al., 2018; Zacharias et al., 2018). Because GSK-3β inhibition was required for alveolosphere formation, our results suggest that upregulation of Wnt/β-catenin downstream target genes are important for AEC2. Wnt5a has been reported to both activate and repress Wnt/β-catenin signaling (van Amerongen et al., 2012); therefore, further studies are required to clarify the specific Wnt as well as downstream signaling mechanisms that are critical for AEC2. Notch2 signaling in AEC2 was shown to be important for alveologenesis using *Notch2*^{cNull} mice (Tsao et al., 2016), and we confirmed the importance of Notch signaling in the generation of alveolospheres. Interestingly, Jagged1 is also required for intestinal organoid formation (Sato et al., 2009); thus, Notch signaling may be conserved among endoderm-derived epithelial cells.

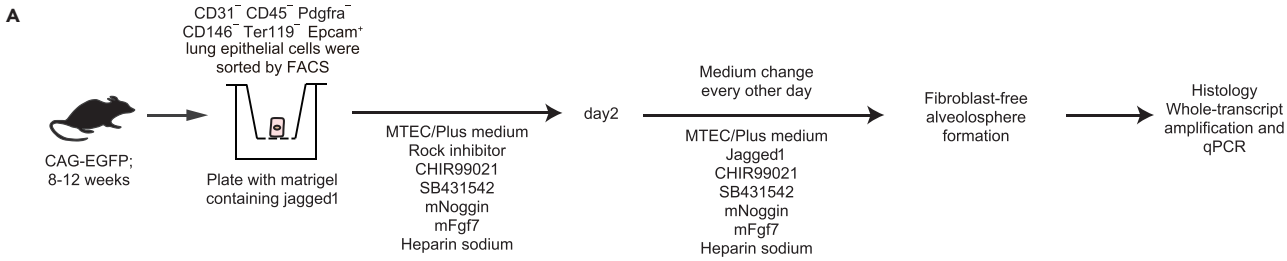
A
CD31⁻ CD45⁻ Pdgfra⁻
CD146⁻ Ter119⁻ Epcam⁺
lung epithelial cells were
sorted by FACS
CAG-EGFP;
8-12 weeks
Plate with matrigel
containing jagged1
MTEC/Plus medium
Rock inhibitor
CHIR99021
SB431542
mNoggin
mFgf7
Heparin sodium
day2
Medium change
every other day
MTEC/Plus medium
Jagged1
CHIR99021
SB431542
mNoggin
mFgf7
Heparin sodium
Fibroblast-free
alveolosphere
formation
Histology
Whole-transcript
amplification and
qPCR

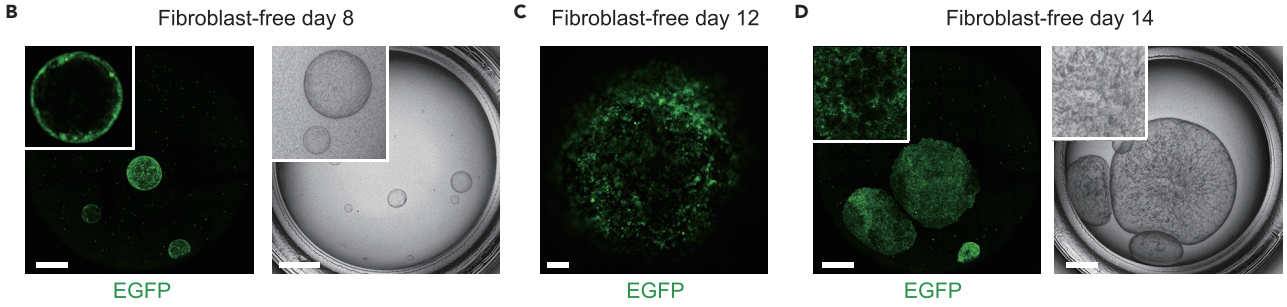
B
Fibroblast-free day 8
C
Fibroblast-free day 12
D
Fibroblast-free day 14
EGFP
EGFP
EGFP

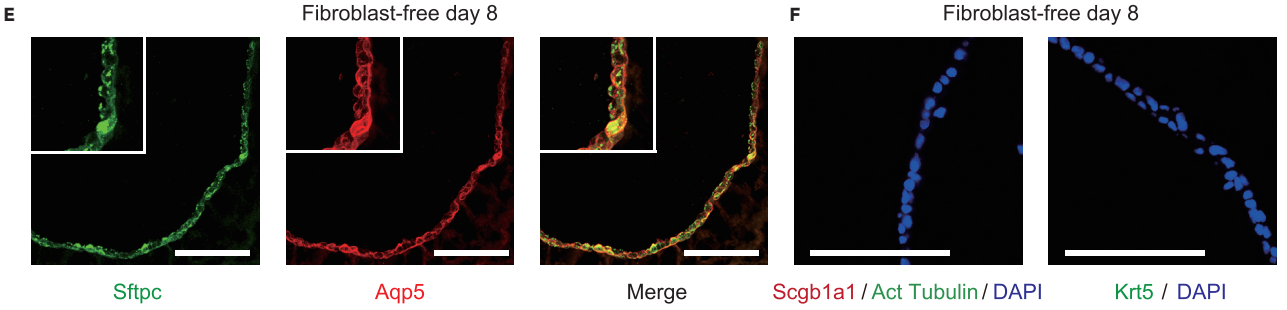
E
Fibroblast-free day 8
F
Fibroblast-free day 8
Sftpc
Aqp5
Merge
Scgb1a1 / Act Tubulin / DAPI
Krt5 / DAPI

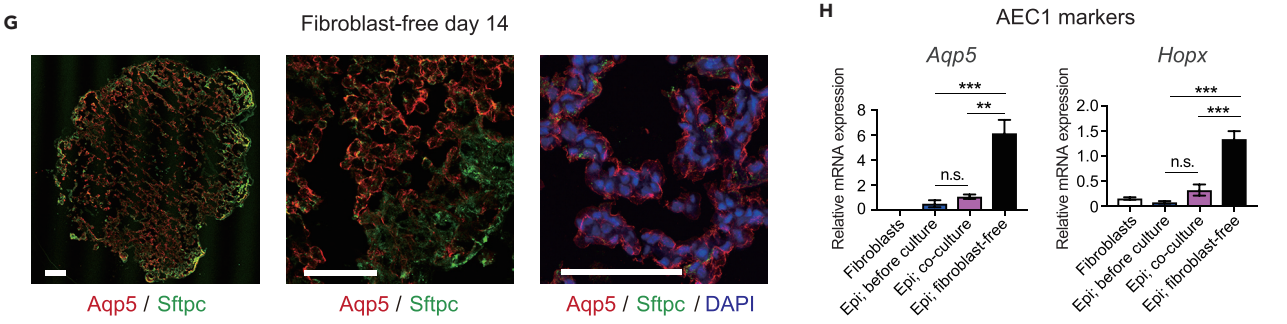
G
Fibroblast-free day 14
H
AEC1 markers
Aqp5
Hopx
Relative mRNA expression
Fibroblasts
Epi; before culture
Epi; co-culture
Epi; fibroblast-free
n.s.
***
**

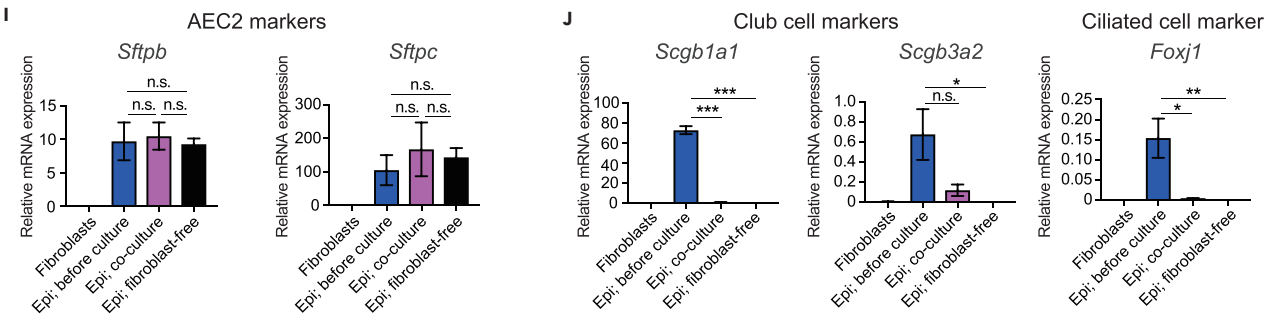
I
AEC2 markers
Sftpb
Sftpc
J
Club cell markers
Scgb1a1
Scgb3a2
Ciliated cell marker
Foxj1
Relative mRNA expression
n.s.
*
**
***

Figure 6. Combination of Fibroblast Ligands and Signaling Pathway Inhibitors Induce the Formation of Fibroblast-Free Alveolospheres

(A) Experimental scheme of the fibroblast-free alveolosphere culture.

(B–D) Representative wells (entire Transwell stored in 24-well plates is shown) from fibroblast-free alveolospheres formation assays on day 8 (B) or 14 (D) and representative fibroblast-free alveolosphere (epithelial cells; EGFP) on day 12 (C). Confocal micrographs (B, left and D, left) and bright-field images (B, right and D, right) are shown.

(E–G) Representative sections of fibroblast-free alveolospheres on day 8 (E and F) and day 14 (G) labeled with antibodies against Aqp5/Sftpc (E and G), Scgb1a1/acetylated tubulin (F left), or Krt5 (F right), showing $Sftpc^+$ $Aqp5^+$ cells on the outside and no cells inside (E) and $Sftpc^+$ AEC2 on the outside and $Aqp5^+$ AEC1 on the inside (G).

(H–J) qPCR analysis of AEC1 (H), AEC2 (I), and non-alveolar epithelial (J) markers using cells obtained from epithelial-fibroblast co-culture (day 14) or fibroblast-free alveolosphere formation assays (day 14). "Fibroblasts" refer to sorted fibroblasts before co-culture and "Epi; before culture" refers to sorted epithelial cells before co-culture. mRNA levels were normalized to that of *Actb*. Data represent mean ± SEM (n = 3 wells for cultured cells and n = 3 animals for sorted cells) and are representative of two independent experiments. *$p < 0.05$, **$p < 0.01$, ***$p < 0.001$ (one-way ANOVA with Tukey's *post hoc* test). Scale bars: 1 mm in B and D; 100 μm in C and E–G. See also Figures S5 and S6.

To examine AEC2, it is essential to culture them *in vitro*. However, there has been no report describing the establishment of passaged cell lines that exhibit morphologic and molecular characteristics of AEC2 (Gonzalez and Dobbs, 2013). Epithelial cell-fibroblast co-cultured alveolospheres are passageable (Barkauskas et al., 2017), but the results obtained from co-culture assays cannot be generalized to AEC2 itself. We established a protocol for passageable fibroblast-free alveolosphere generation that will allow researchers to culture AEC2 for further analysis in the future.

In conclusion, the time course transcriptome analysis of epithelial cells and fibroblasts during alveologenesis and in mature lungs revealed dynamic transcriptional profiles. We identified putative regulators of these processes and generated passageable fibroblast-free alveolospheres using a specific combination of fibroblast ligands and signaling pathway inhibitors. Our results provide a resource for future studies on the molecular mechanisms of lung development.

Limitations of the Study

One of the limitations of our study is that bulk epithelial cells were used for co-culture alveolosphere formation assays. Although nearly 90% of $Epcam^+$ epithelial cells were found to be $Sftpc^+$, the $Epcam^+$ population includes airway cells. For this reason, results obtained using bulk $Epcam^+$ epithelial cells may not be generalizable to AEC2. We sought to overcome this limitation by using purified AEC2 (MHCII-positive) for fibroblast-free alveolosphere assays. Further studies using genetically modified mice that allow direct isolation of $Sftpc^+$ AEC2 are needed to clarify this point. In addition, SAGE-seq included few samples for each time point; therefore, the statistical power might have been low for some of the statistical analyses. Specifically, correlation analysis requires more samples for more biologically meaningful analyses. Use of AEC1 markers *Aqp5* and *Hopx* in qPCR analyses might be another limitation. Although the AEC1 markers have long been used to distinguish AEC1 immunohistochemically (Flodby et al., 2010), in some single cell RNA-sequencing studies, weak mRNA expression of AEC1 markers in AEC2 has been reported (Treutlein et al., 2014).

METHODS

All methods can be found in the accompanying Transparent Methods supplemental file.

DATA AND SOFTWARE AVAILABILITY

Raw data from RNA sequencing have been deposited in the GEO. The GEO accession number for the RNA sequencing data of epithelial cells and fibroblasts from Col1a2-GFP mice reported in this paper is GSE113160 and RNA sequencing data of E13.5, E15.5, P14, and P56 epithelial cells from C57BL/6J mice is GSE109847.

SUPPLEMENTAL INFORMATION

Supplemental Information includes Transparent Methods, six figures, and eight tables and can be found with this article online at https://doi.org/10.1016/j.isci.2018.12.022.

ACKNOWLEDGMENTS

We thank Shun-ichi Fujita and Shin Aoki for technical assistance, Yutaka Inagaki for providing Col1a2-GFP mice, Atsushi Miyawaki for providing Fucci mice, and the University of Tokyo Graduate Program

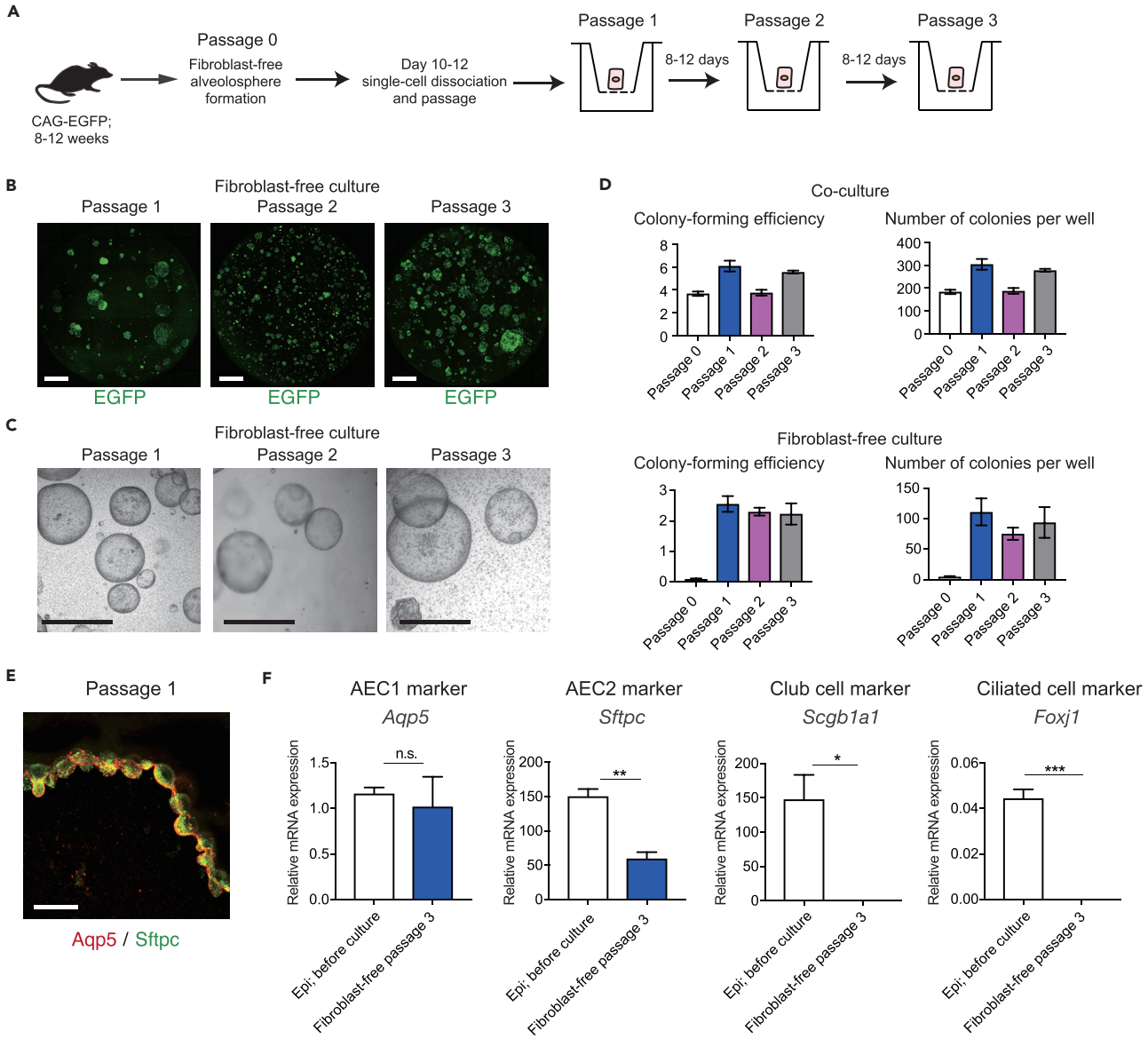

Figure 7. Passage of Fibroblast-Free Alveolospheres as Single-Cell Suspensions

(A) Experimental scheme of fibroblast-free alveolosphere passaging. Colonies were dissociated and 2 × 10^3–5 × 10^3 cells were plated.

(B) Confocal micrographs of representative wells of passaged spheres (epithelial cells; EGFP; entire Transwell stored in 24-well plates is shown) after 8–12 days.

(C) Bright-field images of representative wells of passaged spheres.

(D) Colony-forming efficiency of fibroblast-free and co-cultured alveolospheres. To calculate colony-forming efficiency, all colonies formed in each well were counted and the number of colonies was divided by 5 × 10^3 (for primary cultures and for passaging of co-cultured alveolospheres) or 2 × 10^3–5 × 10^3 (for passaging of fibroblast-free alveolospheres). Colony-forming efficiency of primary fibroblast-free alveolosphere culture (P0) was 0.1% ± 0.02 (5.0 ± 0.9 spheres per well). Fibroblast-free alveolospheres were passaged at least three times without loss of colony-forming efficiency. For P0, n = 12 wells for fibroblast-free culture and n = 9 wells for co-culture pooled from at least two independent cell sorting; for P1, P2, or P3, n = 3 or 4 wells for fibroblast-free culture and n = 6 wells for co-culture pooled from at least two independent passaging procedures.

(E) Representative section of passaged fibroblast-free alveolosphere (passage 1) on day 8 labeled with antibodies against Aqp5/Sftpc.

(F) qPCR analysis of AEC1, AEC2, and non-alveolar epithelial markers using cells obtained from passaged spheres (passage 3, day 8). Data represent mean ± SEM (n = 3 wells for cultured cells and n = 3 animals for sorted cells) and are representative of two independent experiments. mRNA levels were normalized to that of *Actb*. *p < 0.05, **p < 0.01, ***p < 0.001 (unpaired Student's t test [two-tailed]).

Scale bar: 1 mm (B and C), 25 μm (E).

for Leaders in Life Innovation for their assistance with Ion Proton Sequencing. This work was supported by a Grant-in-Aid for Scientific Research on Innovative Areas 17H06392; Grants-in-Aid for Scientific Research (B) 16H05203 and (C) 16K08730; and a Grant-in-Aid for Challenging Research (Exploratory) 17K19546.

AUTHOR CONTRIBUTIONS

K.S. conceived and performed experiments and wrote the manuscript. S.S. conceived and performed SAGE-seq analysis. T.N. performed cell culture. S.H., S.U., S.Y., and K.M. provided expertise and feedback.

DECLARATION OF INTERESTS

The authors declare no competing interests.

Received: May 7, 2018
Revised: August 30, 2018
Accepted: December 20, 2018
Published: January 25, 2019

REFERENCES

Ashburner, M., Ball, C.A., Blake, J.A., Botstein, D., Butler, H., Cherry, J.M., Davis, A.P., Dolinski, K., Dwight, S.S., Eppig, J.T., et al. (2000). Gene ontology: tool for the unification of biology. The Gene Ontology Consortium. Nat. Genet. *25*, 25–29.

Barkauskas, C.E., Chung, M.-I., Fioret, B., Gao, X., Katsura, H., and Hogan, B.L.M. (2017). Lung organoids: current uses and future promise. Development *144*, 986–997.

Barkauskas, C.E., Cronce, M.J., Rackley, C.R., Bowie, E.J., Keene, D.R., Stripp, B.R., Randell, S.H., Noble, P.W., and Hogan, B.L.M. (2013). Type 2 alveolar cells are stem cells in adult lung. J. Clin. Invest. *123*, 3025–3036.

Chao, C.-M., Moiseenko, A., Zimmer, K.-P., and Bellusci, S. (2016). Alveologenesis: key cellular players and fibroblast growth factor 10 signaling. Mol. Cell. Pediatr. *3*, 17.

Chen, H., Matsumoto, K., Brockway, B.L., Rackley, C.R., Liang, J., Lee, J.-H., Jiang, D., Noble, P.W., Randell, S.H., Kim, C.F., et al. (2012). Airway epithelial progenitors are region specific and show differential responses to bleomycin-induced lung injury. Stem Cells *30*, 1948–1960.

De Val, S., Ponticos, M., Antoniv, T.T., Wells, D.J., Abraham, D., Partridge, T., and Bou-Gharios, G. (2002). Identification of the key regions within the mouse pro-alpha 2(I) collagen gene far-upstream enhancer. J. Biol. Chem. *277*, 9286–9292.

Farin, H.F., Jordens, I., Mosa, M.H., Basak, O., Korving, J., Tauriello, D.V.F., de Punder, K., Angers, S., Peters, P.J., Maurice, M.M., et al. (2016). Visualization of a short-range Wnt gradient in the intestinal stem-cell niche. Nature *530*, 340–343.

Flodby, P., Borok, Z., Banfalvi, A., Zhou, B., Gao, D., Minoo, P., Ann, D.K., Morrisey, E.E., and Crandall, E.D. (2010). Directed expression of Cre in alveolar epithelial type 1 cells. Am. J. Respir. Cell Mol. Biol. *43*, 173–178.

Frank, D.B., Peng, T., Zepp, J.A., Snitow, M., Vincent, T.L., Penkala, I.J., Cui, Z., Herriges, M.J., Morley, M.P., Zhou, S., et al. (2016). Emergence of a wave of Wnt signaling that regulates lung alveologenesis by controlling epithelial self-renewal and differentiation. Cell Rep. *17*, 2312–2325.

Gonzalez, R.F., and Dobbs, L.G. (2013). Isolation and culture of alveolar epithelial Type I and Type II cells from rat lungs. Methods Mol. Biol. *945*, 145–159.

Guzy, R.D., Stoilov, I., Elton, T.J., Mecham, R.P., and Ornitz, D.M. (2015). Fibroblast growth factor 2 is required for epithelial recovery, but not for pulmonary fibrosis, in response to bleomycin. Am. J. Respir. Cell Mol. Biol. *52*, 116–128.

Hasegawa, K., Sato, A., Tanimura, K., Uemasu, K., Hamakawa, Y., Fuseya, Y., Sato, S., Muro, S., and Hirai, T. (2017). Fraction of MHCII and EpCAM expression characterizes distal lung epithelial cells for alveolar type 2 cell isolation. Respir. Res. *18*, 150.

Herriges, M., and Morrisey, E.E. (2014). Lung development: orchestrating the generation and regeneration of a complex organ. Development *141*, 502–513.

Hogan, B.L.M., Barkauskas, C.E., Chapman, H.A., Epstein, J.A., Jain, R., Hsia, C.C.W., Niklason, L., Calle, E., Le, A., Randell, S.H., et al. (2014). Repair and regeneration of the respiratory system: complexity, plasticity, and mechanisms of lung stem cell function. Cell Stem Cell *15*, 123–138.

Jain, R., Barkauskas, C.E., Takeda, N., Bowie, E.J., Aghajanian, H., Wang, Q., Padmanabhan, A., Manderfield, L.J., Gupta, M., Li, D., et al. (2015). Plasticity of Hopx(+) type I alveolar cells to regenerate type II cells in the lung. Nat. Commun. *6*, 6727.

Kanehisa, M., Furumichi, M., Tanabe, M., Sato, Y., and Morishima, K. (2017). KEGG: new perspectives on genomes, pathways, diseases and drugs. Nucleic Acids Res. *45*, D353–D361.

Kim, C.F.B., Jackson, E.L., Woolfenden, A.E., Lawrence, S., Babar, I., Vogel, S., Crowley, D., Bronson, R.T., and Jacks, T. (2005). Identification of bronchioalveolar stem cells in normal lung and lung cancer. Cell *121*, 823–835.

Lee, J.-H., Tammela, T., Hofree, M., Choi, J., Marjanovic, N.D., Han, S., Canner, D., Wu, K., Paschini, M., Bhang, D.H., et al. (2017). Anatomically and functionally distinct lung mesenchymal populations marked by Lgr5 and Lgr6. Cell *170*, 1149–1163.e12.

McCulley, D., Wienhold, M., and Sun, X. (2015). The pulmonary mesenchyme directs lung development. Curr. Opin. Genet. Dev. *32*, 98–105.

McGowan, S.E., Harvey, C.S., and Jackson, S.K. (1995). Retinoids, retinoic acid receptors, and cytoplasmic retinoid binding proteins in perinatal rat lung fibroblasts. Am. J. Physiol. *269*, L463–L472.

McQualter, J.L., and Bertoncello, I. (2012). Concise review: Deconstructing the lung to reveal its regenerative potential. Stem Cells *30*, 811–816.

Nabhan, A., Brownfield, D.G., Harbury, P.B., Krasnow, M.A., and Desai, T.J. (2018). Single-cell Wnt signaling niches maintain stemness of alveolar type 2 cells. Science *137*, eaam6603.

Ornitz, D.M., and Itoh, N. (2015). The fibroblast growth factor signaling pathway. Wiley Interdiscip. Rev. Dev. Biol. *4*, 215–266.

Peng, T., Frank, D.B., Kadzik, R.S., Morley, M.P., Rathi, K.S., Wang, T., Zhou, S., Cheng, L., Lu, M.M., and Morrisey, E.E. (2015). Hedgehog actively maintains adult lung quiescence and regulates repair and regeneration. Nature *526*, 578–582.

Plotnikov, A., Zehorai, E., Procaccia, S., and Seger, R. (2011). The MAPK cascades: signaling components, nuclear roles and mechanisms of nuclear translocation. Biochim. Biophys. Acta *1813*, 1619–1633.

Sakaue-Sawano, A., Kurokawa, H., Morimura, T., Hanyu, A., Hama, H., Osawa, H., Kashiwagi, S., Fukami, K., Miyata, T., Miyoshi, H., et al. (2008). Visualizing spatiotemporal dynamics of multicellular cell-cycle progression. Cell *132*, 487–498.

Sato, T., Vries, R.G., Snippert, H.J., van de Wetering, M., Barker, N., Stange, D.E., van Es, J.H., Abo, A., Kujala, P., Peters, P.J., et al. (2009). Single Lgr5 stem cells build crypt-villus structures in vitro without a mesenchymal niche. Nature *459*, 262–265.

Schultz, C.J., Torres, E., Londos, C., and Torday, J.S. (2002). Role of adipocyte differentiation-related protein in surfactant phospholipid synthesis by type II cells. Am. J. Physiol. Lung Cell Mol. Physiol. *283*, L288–L296.

Sharan, R., Maron-Katz, A., and Shamir, R. (2003). CLICK and EXPANDER: a system for clustering and visualizing gene expression data. Bioinformatics *19*, 1787–1799.

Shy, B.R., Wu, C.-I., Khramtsova, G.F., Zhang, J.Y., Olopade, O.I., Goss, K.H., and Merrill, B.J. (2013). Regulation of Tcf7l1 DNA binding and protein stability as principal mechanisms of Wnt/β-catenin signaling. Cell Rep. *4*, 1–9.

Sun, J., Nishiyama, T., Shimizu, K., and Kadota, K. (2013). TCC: an R package for comparing tag count data with robust normalization strategies. BMC Bioinformatics *14*, 219.

Tomura, M., Sakaue-Sawano, A., Mori, Y., Takase-Utsugi, M., Hata, A., Ohtawa, K., Kanagawa, O., and Miyawaki, A. (2013). Contrasting quiescent G0 phase with mitotic cell cycling in the mouse immune system. PLoS One *8*, e73801.

Treutlein, B., Brownfield, D.G., Wu, A.R., Neff, N.F., Mantalas, G.L., Espinoza, F.H., Desai, T.J., Krasnow, M.A., and Quake, S.R. (2014). Reconstructing lineage hierarchies of the distal lung epithelium using single-cell RNA-seq. Nature *509*, 371–375.

Tsao, P.-N., Matsuoka, C., Wei, S.-C., Sato, A., Sato, S., Hasegawa, K., Chen, H.-K., Ling, T.-Y., Mori, M., Cardoso, W.V., et al. (2016). Epithelial Notch signaling regulates lung alveolar morphogenesis and airway epithelial integrity. Proc. Natl. Acad. Sci. U S A *113*, 8242–8247.

Tsukui, T., Ueha, S., Abe, J., Hashimoto, S.-I., Shichino, S., Shimaoka, T., Shand, F.H.W., Arakawa, Y., Oshima, K., Hattori, M., et al. (2013). Qualitative rather than quantitative changes are hallmarks of fibroblasts in bleomycin-induced pulmonary fibrosis. Am. J. Pathol. *183*, 758–773.

van Amerongen, R., Fuerer, C., Mizutani, M., and Nusse, R. (2012). Wnt5a can both activate and repress Wnt/β-catenin signaling during mouse embryonic development. Dev. Biol. *369*, 101–114.

Volckaert, T., and De Langhe, S.P. (2015). Wnt and FGF mediated epithelial-mesenchymal crosstalk during lung development. Dev. Dyn. *244*, 342–366.

Yamazaki, S., Ema, H., Karlsson, G., Yamaguchi, T., Miyoshi, H., Shioda, S., Taketo, M.M., Karlsson, S., Iwama, A., and Nakauchi, H. (2011). Nonmyelinating Schwann cells maintain hematopoietic stem cell hibernation in the bone marrow niche. Cell *147*, 1146–1158.

Zacharias, W.J., Frank, D.B., Zepp, J.A., Morley, M.P., Alkhaleel, F.A., Kong, J., Zhou, S., Cantu, E., and Morrisey, E.E. (2018). Regeneration of the lung alveolus by an evolutionarily conserved epithelial progenitor. Nature *143*, 3639.

Zepp, J.A., Zacharias, W.J., Frank, D.B., Cavanaugh, C.A., Zhou, S., Morley, M.P., and Morrisey, E.E. (2017). Distinct mesenchymal lineages and niches promote epithelial self-renewal and myofibrogenesis in the lung. Cell *170*, 1134–1148.e10.

Zhang, S., Loch, A.J., Radtke, F., Egan, S.E., and Xu, K. (2013). Jagged1 is the major regulator of Notch-dependent cell fate in proximal airways. Dev. Dyn. *242*, 678–686.

ISCI, Volume *11*

Supplemental Information

Mesenchymal-Epithelial Interactome Analysis Reveals Essential Factors Required for Fibroblast-Free Alveolosphere Formation

Kazushige Shiraishi, Shigeyuki Shichino, Satoshi Ueha, Takuya Nakajima, Shinichi Hashimoto, Satoshi Yamazaki, and Kouji Matsushima

Figure S1

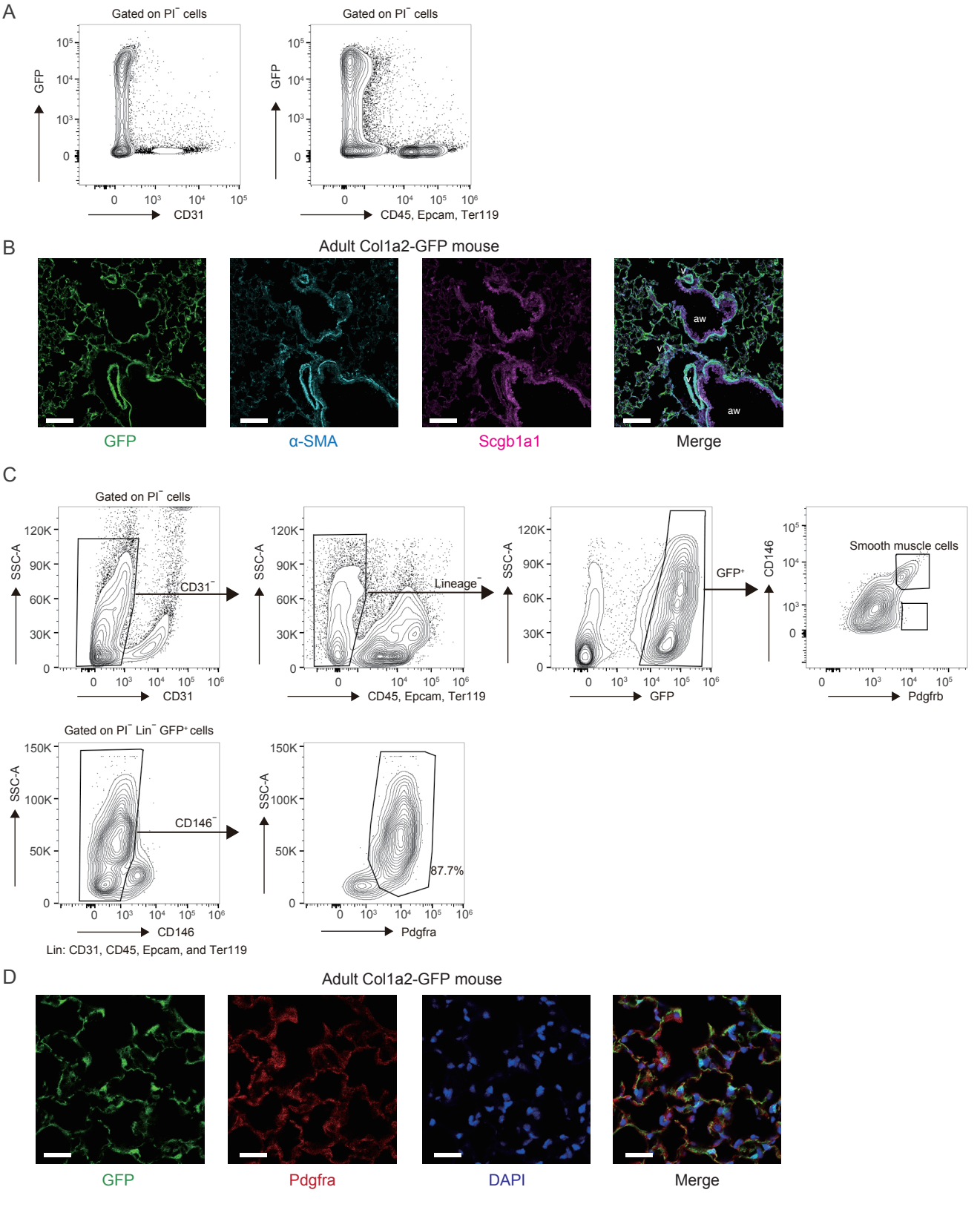
A
Gated on PI⁻ cells
GFP
CD31
Gated on PI⁻ cells
GFP
CD45, Epcam, Ter119
B
Adult Col1a2-GFP mouse
GFP
α-SMA
Scgb1a1
Merge
v
aw
C
Gated on PI⁻ cells
SSC-A
CD31⁻
CD31
Lineage⁻
CD45, Epcam, Ter119
GFP⁺
GFP
CD146
Smooth muscle cells
Pdgfrb
Gated on PI⁻ Lin⁻ GFP⁺ cells
CD146⁻
CD146
87.7%
Pdgfra
Lin: CD31, CD45, Epcam, and Ter119
D
Adult Col1a2-GFP mouse
GFP
Pdgfra
DAPI
Merge

Figure S1. Immunohistochemical and flow cytometry analyses of GFP$^+$ cells in the lungs of Col1a2-GFP mice, related to Figure 1. (A) Representative gating plots of P56 adult Col1a2-GFP mice are shown. The GFP$^+$ population did not include CD31$^+$ endothelial cells, CD45$^+$ blood cells, Epcam$^+$ epithelial cells, or Ter119$^+$ erythrocytes. (B) Representative lung sections from P56 Col1a2-GFP mice were stained for Scgb1a1 (magenta) and α-SMA (cyan). (C) Gating scheme for characterization of GFP$^+$ population in the lungs of Col1a2-GFP mice. Representative plots of P56 adult Col1a2-GFP mice are shown. The GFP$^+$ population did not include CD146$^-$ Pdgfrb$^+$ mesenchymal population, but included CD146$^+$ smooth muscle cells, Pdgfra$^+$ alveolar fibroblasts, and Pdgfra$^-$ fibroblasts. (D) Representative lung sections from P56 Col1a2-GFP mice were immunolabeled for Pdgfra (red) and stained with 4',6-diamidino-2-phenylindole (blue). Scale bars: 100 μm (B), 25 μm (D). aw, airway; v, blood vessel.

Figure S2

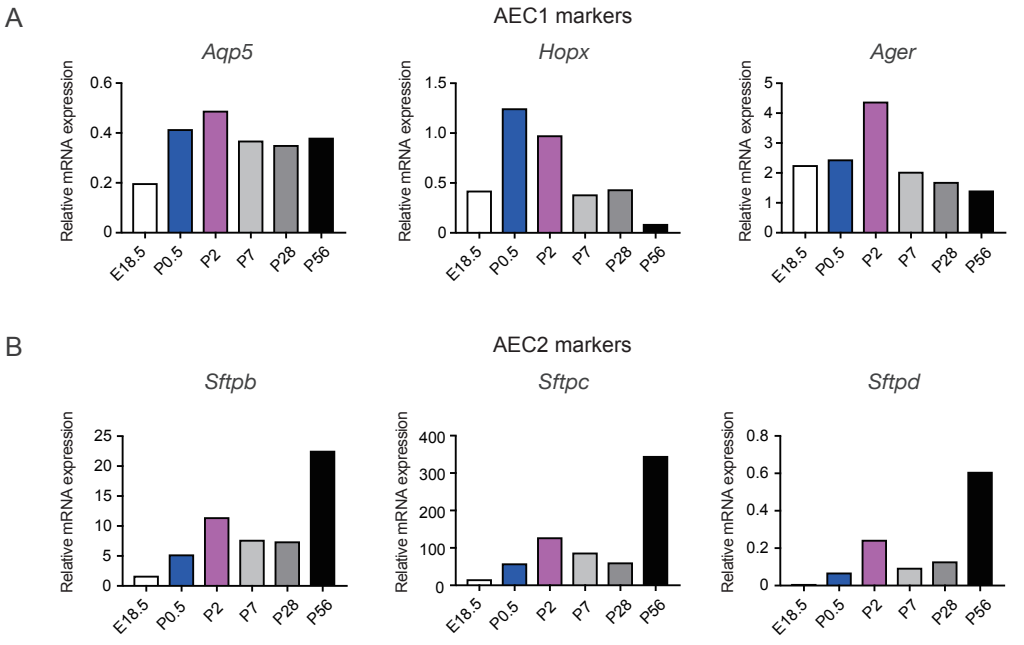

Figure S2. qPCR validation of transcriptome data, related to Figure 1. (A, B) qPCR of type 1 (A) and type 2 (B) alveolar epithelial cell marker genes using cells obtained from transcriptome analyses. Data represent mean of two biological replicates obtained from two animals. mRNA levels were normalized to that of *Gapdh*.

Figure S3

A

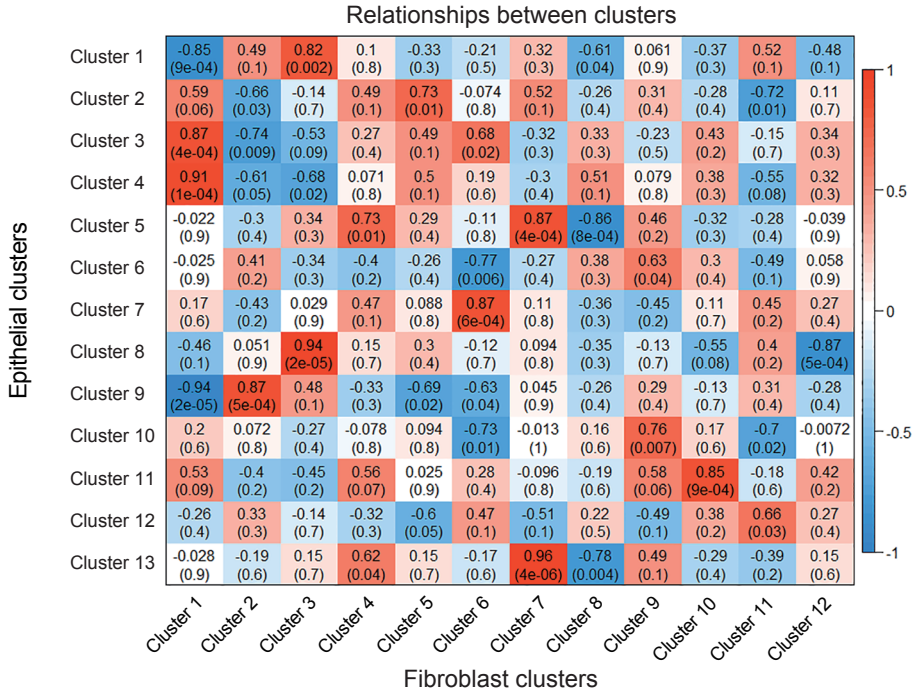
Relationships between clusters
Epithelial clusters
Cluster 1 -0.85 (9e-04) 0.49 (0.1) 0.82 (0.002) 0.1 (0.8) -0.33 (0.3) -0.21 (0.5) 0.32 (0.3) -0.61 (0.04) 0.061 (0.9) -0.37 (0.3) 0.52 (0.1) -0.48 (0.1)
Cluster 2 0.59 (0.06) -0.66 (0.03) -0.14 (0.7) 0.49 (0.1) 0.73 (0.01) -0.074 (0.8) 0.52 (0.1) -0.26 (0.4) 0.31 (0.4) -0.28 (0.4) -0.72 (0.01) 0.11 (0.7)
Cluster 3 0.87 (4e-04) -0.74 (0.009) -0.53 (0.09) 0.27 (0.4) 0.49 (0.1) 0.68 (0.02) -0.32 (0.3) 0.33 (0.3) -0.23 (0.5) 0.43 (0.2) -0.15 (0.7) 0.34 (0.3)
Cluster 4 0.91 (1e-04) -0.61 (0.05) -0.68 (0.02) 0.071 (0.8) 0.5 (0.1) 0.19 (0.6) -0.3 (0.4) 0.51 (0.1) 0.079 (0.8) 0.38 (0.3) -0.55 (0.08) 0.32 (0.3)
Cluster 5 -0.022 (0.9) -0.3 (0.4) 0.34 (0.3) 0.73 (0.01) 0.29 (0.4) -0.11 (0.8) 0.87 (4e-04) -0.86 (8e-04) 0.46 (0.2) -0.32 (0.3) -0.28 (0.4) -0.039 (0.9)
Cluster 6 -0.025 (0.9) 0.41 (0.2) -0.34 (0.3) -0.4 (0.2) -0.26 (0.4) -0.77 (0.006) -0.27 (0.4) 0.38 (0.3) 0.63 (0.04) 0.3 (0.4) -0.49 (0.1) 0.058 (0.9)
Cluster 7 0.17 (0.6) -0.43 (0.2) 0.029 (0.9) 0.47 (0.1) 0.088 (0.8) 0.87 (6e-04) 0.11 (0.8) -0.36 (0.3) -0.45 (0.2) 0.11 (0.7) 0.45 (0.2) 0.27 (0.4)
Cluster 8 -0.46 (0.1) 0.051 (0.9) 0.94 (2e-05) 0.15 (0.7) 0.3 (0.4) -0.12 (0.7) 0.094 (0.8) -0.35 (0.3) -0.13 (0.7) -0.55 (0.08) 0.4 (0.2) -0.87 (5e-04)
Cluster 9 -0.94 (2e-05) 0.87 (5e-04) 0.48 (0.1) -0.33 (0.3) -0.69 (0.02) -0.63 (0.04) 0.045 (0.9) -0.26 (0.4) 0.29 (0.4) -0.13 (0.7) 0.31 (0.4) -0.28 (0.4)
Cluster 10 0.2 (0.6) 0.072 (0.8) -0.27 (0.4) -0.078 (0.8) 0.094 (0.8) -0.73 (0.01) -0.013 (1) 0.16 (0.6) 0.76 (0.007) 0.17 (0.6) -0.7 (0.02) -0.0072 (1)
Cluster 11 0.53 (0.09) -0.4 (0.2) -0.45 (0.2) 0.56 (0.07) 0.025 (0.9) 0.28 (0.4) -0.096 (0.8) -0.19 (0.6) 0.58 (0.06) 0.85 (9e-04) -0.18 (0.6) 0.42 (0.2)
Cluster 12 -0.26 (0.4) 0.33 (0.3) -0.14 (0.7) -0.32 (0.3) -0.6 (0.05) 0.47 (0.1) -0.51 (0.1) 0.22 (0.5) -0.49 (0.1) 0.38 (0.2) 0.66 (0.03) 0.27 (0.4)
Cluster 13 -0.028 (0.9) -0.19 (0.6) 0.15 (0.7) 0.62 (0.04) 0.15 (0.7) -0.17 (0.6) 0.96 (4e-06) -0.78 (0.004) 0.49 (0.1) -0.29 (0.4) -0.39 (0.2) 0.15 (0.6)
Cluster 1 Cluster 2 Cluster 3 Cluster 4 Cluster 5 Cluster 6 Cluster 7 Cluster 8 Cluster 9 Cluster 10 Cluster 11 Cluster 12
Fibroblast clusters
1
0.5
0
-0.5
-1

B

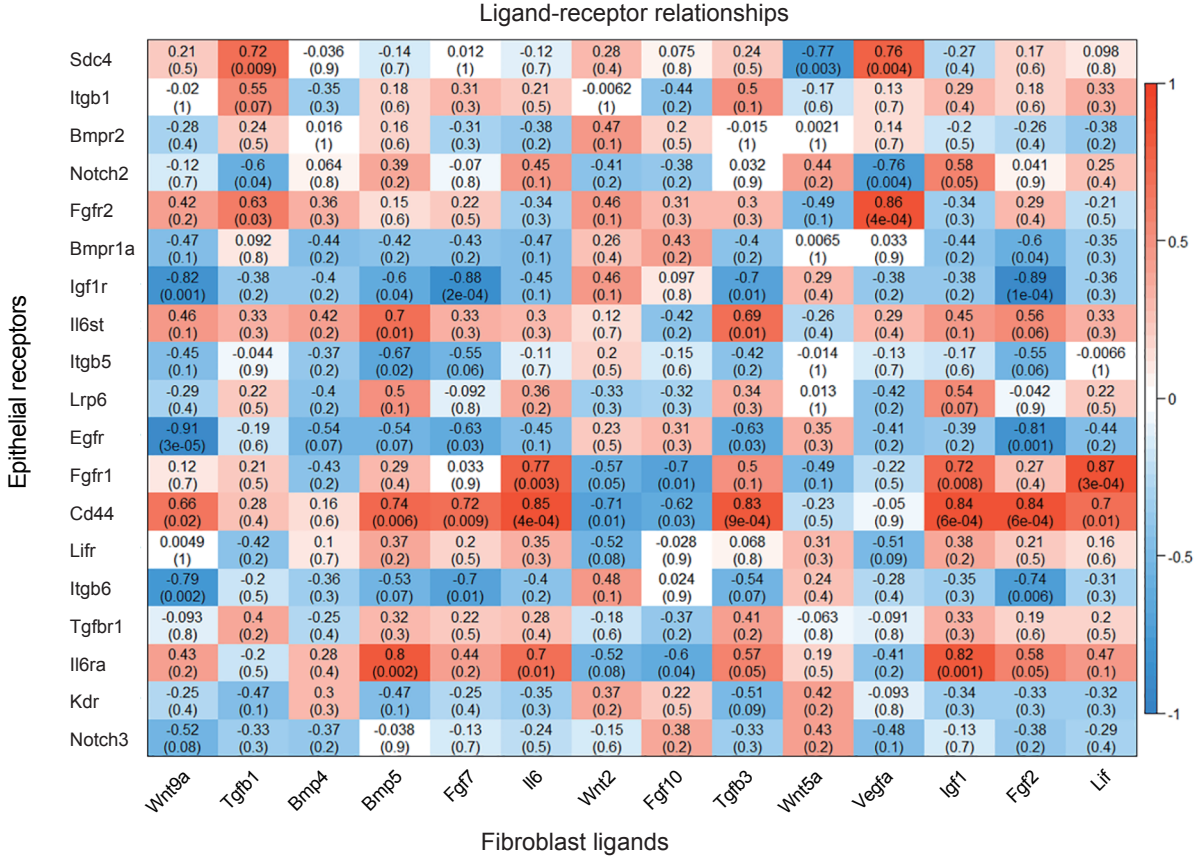
Ligand-receptor relationships
Epithelial receptors
Sdc4 0.21 (0.5) 0.72 (0.009) -0.036 (0.9) -0.14 (0.7) 0.012 (1) -0.12 (0.7) 0.28 (0.4) 0.075 (0.8) 0.24 (0.5) -0.77 (0.003) 0.76 (0.004) -0.27 (0.4) 0.17 (0.6) 0.098 (0.8)
Itgb1 -0.02 (1) 0.55 (0.07) -0.35 (0.3) 0.18 (0.6) 0.31 (0.3) 0.21 (0.5) -0.0062 (1) -0.44 (0.2) 0.5 (0.1) -0.17 (0.6) 0.13 (0.7) 0.29 (0.4) 0.18 (0.6) 0.33 (0.3)
Bmpr2 -0.28 (0.4) 0.24 (0.5) 0.016 (1) 0.16 (0.6) -0.31 (0.3) -0.38 (0.2) 0.47 (0.1) 0.2 (0.5) -0.015 (1) 0.0021 (1) 0.14 (0.7) -0.2 (0.5) -0.26 (0.4) -0.38 (0.2)
Notch2 -0.12 (0.7) -0.6 (0.04) 0.064 (0.8) 0.39 (0.2) -0.07 (0.8) 0.45 (0.1) -0.41 (0.2) -0.38 (0.2) 0.032 (0.9) 0.44 (0.2) -0.76 (0.004) 0.58 (0.05) 0.041 (0.9) 0.25 (0.4)
Fgfr2 0.42 (0.2) 0.63 (0.03) 0.36 (0.3) 0.15 (0.6) 0.22 (0.5) -0.34 (0.3) 0.46 (0.1) 0.31 (0.3) 0.3 (0.3) -0.49 (0.1) 0.86 (4e-04) -0.34 (0.3) 0.29 (0.4) -0.21 (0.5)
Bmpr1a -0.47 (0.1) 0.092 (0.8) -0.44 (0.2) -0.42 (0.2) -0.43 (0.2) -0.47 (0.1) 0.26 (0.4) 0.43 (0.2) -0.4 (0.2) 0.0065 (1) 0.033 (0.9) -0.44 (0.2) -0.6 (0.04) -0.35 (0.3)
Igf1r -0.82 (0.001) -0.38 (0.2) -0.4 (0.2) -0.6 (0.04) -0.88 (2e-04) -0.45 (0.1) 0.46 (0.1) 0.097 (0.8) -0.7 (0.01) 0.29 (0.4) -0.38 (0.2) -0.38 (0.2) -0.89 (1e-04) -0.36 (0.3)
Il6st 0.46 (0.1) 0.33 (0.3) 0.42 (0.2) 0.7 (0.01) 0.33 (0.3) 0.3 (0.3) 0.12 (0.7) -0.42 (0.2) 0.69 (0.01) -0.26 (0.4) 0.29 (0.4) 0.45 (0.1) 0.56 (0.06) 0.33 (0.3)
Itgb5 -0.45 (0.1) -0.044 (0.9) -0.37 (0.2) -0.67 (0.02) -0.55 (0.06) -0.11 (0.7) 0.2 (0.5) -0.15 (0.6) -0.42 (0.2) -0.014 (1) -0.13 (0.7) -0.17 (0.6) -0.55 (0.06) -0.0066 (1)
Lrp6 -0.29 (0.4) 0.22 (0.5) -0.4 (0.2) 0.5 (0.1) -0.092 (0.8) 0.36 (0.2) -0.33 (0.3) -0.32 (0.3) 0.34 (0.3) 0.013 (1) -0.42 (0.2) 0.54 (0.07) -0.042 (0.9) 0.22 (0.5)
Egfr -0.91 (3e-05) -0.19 (0.6) -0.54 (0.07) -0.54 (0.07) -0.63 (0.03) -0.45 (0.1) 0.23 (0.5) 0.31 (0.3) -0.63 (0.03) 0.35 (0.3) -0.41 (0.2) -0.39 (0.2) -0.81 (0.001) -0.44 (0.2)
Fgfr1 0.12 (0.7) 0.21 (0.5) -0.43 (0.2) 0.29 (0.4) 0.033 (0.9) 0.77 (0.003) -0.57 (0.05) -0.7 (0.01) 0.5 (0.1) -0.49 (0.1) -0.22 (0.5) 0.72 (0.008) 0.27 (0.4) 0.87 (3e-04)
Cd44 0.66 (0.02) 0.28 (0.4) 0.16 (0.6) 0.74 (0.006) 0.72 (0.009) 0.85 (4e-04) -0.71 (0.01) -0.62 (0.03) 0.83 (9e-04) -0.23 (0.5) -0.05 (0.9) 0.84 (6e-04) 0.84 (6e-04) 0.7 (0.01)
Lifr 0.0049 (1) -0.42 (0.2) 0.1 (0.7) 0.37 (0.2) 0.2 (0.5) 0.35 (0.3) -0.52 (0.08) -0.028 (0.9) 0.068 (0.8) 0.31 (0.3) -0.51 (0.09) 0.38 (0.2) 0.21 (0.5) 0.16 (0.6)
Itgb6 -0.79 (0.002) -0.2 (0.5) -0.36 (0.3) -0.53 (0.07) -0.7 (0.01) -0.4 (0.2) 0.48 (0.1) 0.024 (0.9) -0.54 (0.07) 0.24 (0.4) -0.28 (0.4) -0.35 (0.3) -0.74 (0.006) -0.31 (0.3)
Tgfbr1 -0.093 (0.8) 0.4 (0.2) -0.25 (0.4) 0.32 (0.3) 0.22 (0.5) 0.28 (0.4) -0.18 (0.6) -0.37 (0.2) 0.41 (0.2) -0.063 (0.8) -0.091 (0.8) 0.33 (0.3) 0.19 (0.6) 0.2 (0.5)
Il6ra 0.43 (0.2) -0.2 (0.5) 0.28 (0.4) 0.8 (0.002) 0.44 (0.2) 0.7 (0.01) -0.52 (0.08) -0.6 (0.04) 0.57 (0.05) 0.19 (0.5) -0.41 (0.2) 0.82 (0.001) 0.58 (0.05) 0.47 (0.1)
Kdr -0.25 (0.4) -0.47 (0.1) 0.3 (0.3) -0.47 (0.1) -0.25 (0.4) -0.35 (0.3) 0.37 (0.2) 0.22 (0.5) -0.51 (0.09) 0.42 (0.2) -0.093 (0.8) -0.34 (0.3) -0.33 (0.3) -0.32 (0.3)
Notch3 -0.52 (0.08) -0.33 (0.3) -0.37 (0.2) -0.038 (0.9) -0.13 (0.7) -0.24 (0.5) -0.15 (0.6) 0.38 (0.2) -0.33 (0.3) 0.43 (0.2) -0.48 (0.1) -0.13 (0.7) -0.38 (0.2) -0.29 (0.4)
Wnt9a Tgfb1 Bmp4 Bmp5 Fgf7 Il6 Wnt2 Fgf10 Tgfb3 Wnt5a Vegfa Igf1 Fgf2 Lif
Fibroblast ligands
1
0.5
0
-0.5
-1

Figure S3. Correlation analysis of transcriptome data, related to Figures 2 and 3.
(A) Correlations between CLICK-identified gene clusters. (B) Correlations between fibroblast-derived ligands and epithelial-derived receptors. Pearson's correlation coefficient (top) and associated Student asymptotic P value for correlation (bottom) are shown.

Figure S4

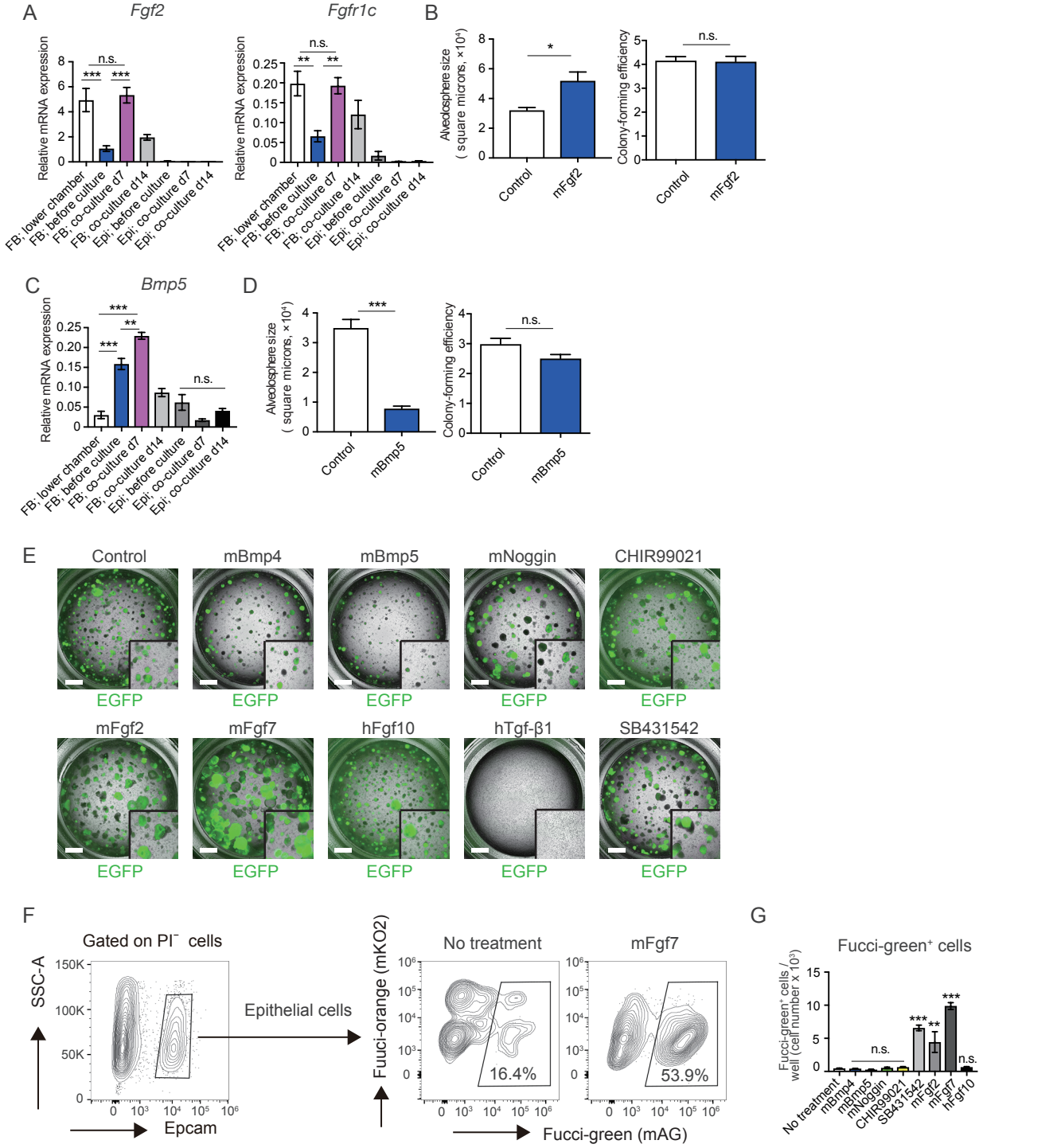
A
Fgf2
Fgfr1c
Relative mRNA expression
n.s.
***
**
FB; lower chamber
FB; before culture
FB; co-culture d7
FB; co-culture d14
Epi; before culture
Epi; co-culture d7
Epi; co-culture d14
B
Alveolosphere size (square microns, ×10⁴)
Colony-forming efficiency
*
Control
mFgf2
C
Bmp5
D
mBmp5
E
Control
mBmp4
mBmp5
mNoggin
CHIR99021
mFgf2
mFgf7
hFgf10
hTgf-β1
SB431542
EGFP
F
Gated on PI⁻ cells
SSC-A
Epcam
Epithelial cells
No treatment
mFgf7
Fucci-orange (mKO2)
Fucci-green (mAG)
16.4%
53.9%
G
Fucci-green⁺ cells
Fucci-green⁺ cells / well (cell number x 10³)

Figure S4. Additional qPCR analysis of Fgf/Bmp signaling and analysis of colony-forming efficiency and proliferative capacity in co-culture assays, related to Figure 5. (A, C) qPCR of *Fgf2* and *Fgfr1c* (A) and *Bmp5* (C) using cells obtained from epithelial-fibroblasts co-culture assays. (n = 3 wells for cultured cells and n = 3 animals for sorted cells). The data are representative of two independent experiments. mRNA levels were normalized to that of *Actb*. (B, D) Fgf2 (B) or Bmp5 (D) was added to the co-culture medium and organoid size as well as colony-forming efficiency was calculated after 14 days. Sphere size was averaged for alveolospheres in each well. To calculate colony-forming efficiency, all colonies formed in each well were counted and the number of colonies was divided by 5×10^3 (epithelial cells plated). Data are shown for n = 3 wells and are representative of two independent experiments. (E) Representative merged images of the co-culture assays. Entire Transwell stored in 24-well plate is shown. (F) Gating scheme for proliferation assays showing Fucci-green positive cells following treatment with mFgf7. (G) Number of Fucci-green positive cells per well after 4 or 5 days of culture. Data represent mean ± SEM (n = 3 wells) and are representative of two independent experiments. *P < 0.05, **P < 0.01, ***P < 0.001 (one-way ANOVA with Tukey's post-hoc test or Student's t test). Scale bar: 1 mm.

Figure S5

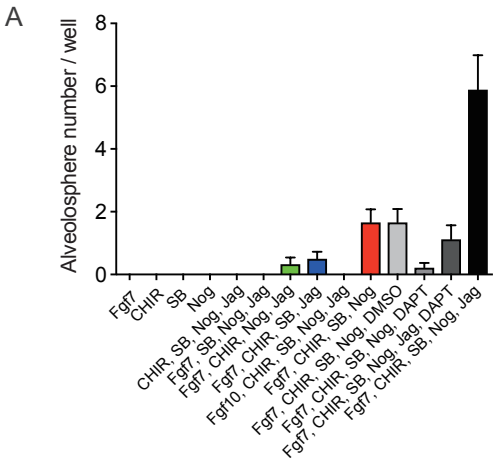
A
Alveolosphere number / well
0
2
4
6
8
Fgf7
CHIR
SB
Nog
Jag
CHIR, SB, Nog, Jag
Fgf7, SB, Nog, Jag
Fgf7, CHIR, Nog, Jag
Fgf7, CHIR, SB, Jag
Fgf7, CHIR, SB, Nog, Jag
Fgf10, CHIR, SB, Nog
Fgf7, CHIR, SB, Nog
Fgf7, CHIR, SB, Nog, DMSO
Fgf7, CHIR, SB, Nog, DAPT
Fgf7, CHIR, SB, Nog, Jag, DAPT
Fgf7, CHIR, SB, Nog, Jag

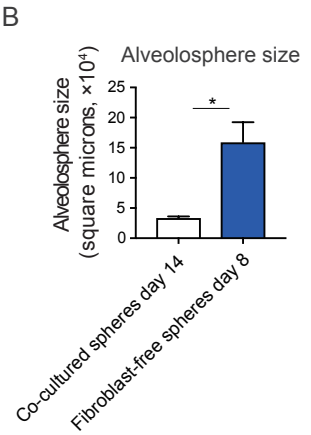
B
Alveolosphere size
Alveolosphere size (square microns, ×10⁴)
0
5
10
15
20
25
*
Co-cultured spheres day 14
Fibroblast-free spheres day 8

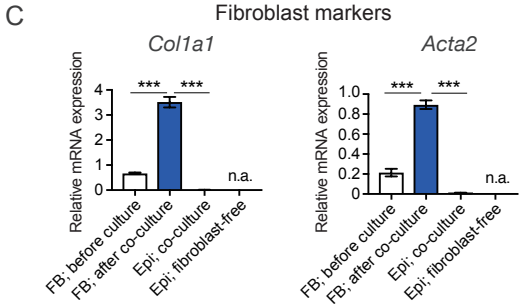
C
Fibroblast markers
Col1a1
Acta2
Relative mRNA expression
***
***
n.a.
FB; before culture
FB; after co-culture
Epi; co-culture
Epi; fibroblast-free

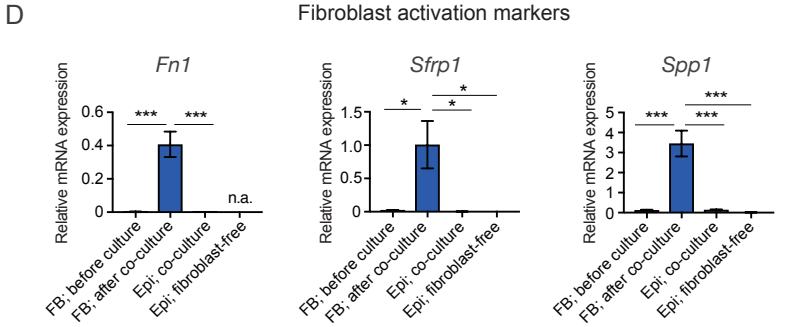
D
Fibroblast activation markers
Fn1
Sfrp1
Spp1
Relative mRNA expression
n.a.
FB; before culture
FB; after co-culture
Epi; co-culture
Epi; fibroblast-free

Figure S5. Assessment of sphere size and sphere generation in response to different molecule combinations, and qPCR detection of fibroblast and fibroblast activation markers in the fibroblast-free alveolosphere assay, related to Figure 6. (A) Alveolosphere number per well (culture day 8) under culture conditions with several combinations of molecules. Data represent mean ± SEM pooled from two or three independent experiments (n = 6–9 wells). (B) Alveolosphere size of co-cultured alveolospheres on day 14 and fibroblast-free alveolospheres on day 8. Sphere size was averaged for alveolospheres in each well (n = 3 wells). The data are representative of two independent experiments. (C, D) qPCR analysis of fibroblast markers (C) and fibroblast activation markers (D) using cells obtained from epithelial–fibroblasts co-cultures or fibroblast-free alveolospheres. mRNA levels were normalized to that of *Actb*. Data represent mean ± SEM (n = 3 wells for cultured cells and n = 3 animals for sorted cells) and are representative of two independent experiments. *P < 0.05, ***P < 0.001 (one-way ANOVA with Tukey's post-hoc test or Student's t test). CHIR, CHIR99021; DMSO, dimethylsulfoxide; Jag, Jagged-1; Nog, mNoggin; SB, SB431542.

Figure S6

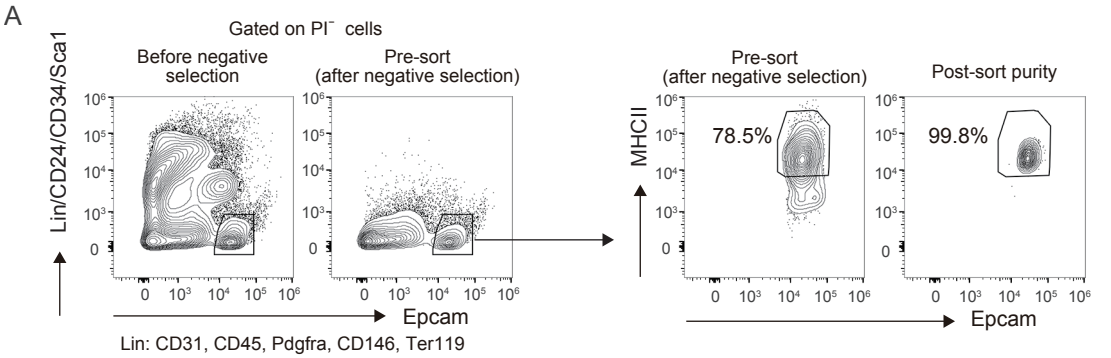
A
Gated on PI⁻ cells
Before negative selection
Pre-sort (after negative selection)
Lin/CD24/CD34/Sca1
Epcam
Lin: CD31, CD45, Pdgfra, CD146, Ter119
Pre-sort (after negative selection)
Post-sort purity
MHCII
78.5%
99.8%
Epcam

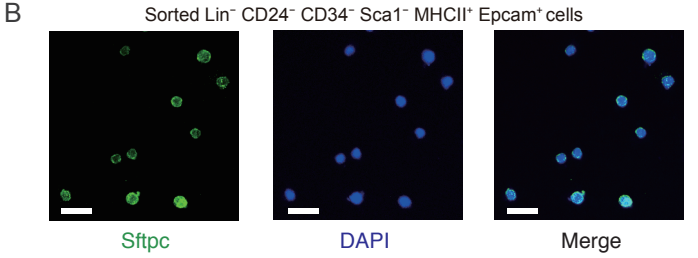
B
Sorted Lin⁻ CD24⁻ CD34⁻ Sca1⁻ MHCII⁺ Epcam⁺ cells
Sftpc
DAPI
Merge

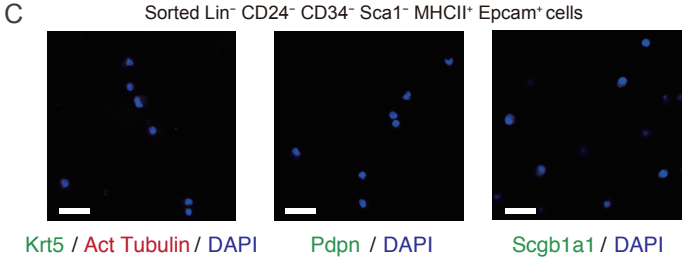
C
Sorted Lin⁻ CD24⁻ CD34⁻ Sca1⁻ MHCII⁺ Epcam⁺ cells
Krt5 / Act Tubulin / DAPI
Pdpn / DAPI
Scgb1a1 / DAPI

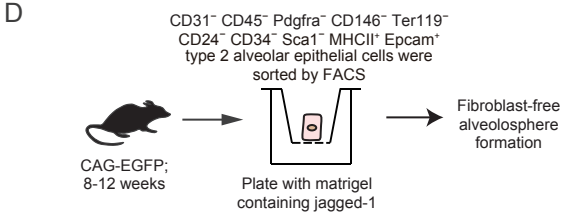
D
CD31⁻ CD45⁻ Pdgfra⁻ CD146⁻ Ter119⁻
CD24⁻ CD34⁻ Sca1⁻ MHCII⁺ Epcam⁺
type 2 alveolar epithelial cells were
sorted by FACS
CAG-EGFP;
8-12 weeks
Plate with matrigel
containing jagged-1
Fibroblast-free
alveolosphere
formation

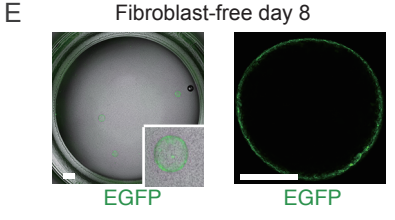
E
Fibroblast-free day 8
EGFP
EGFP

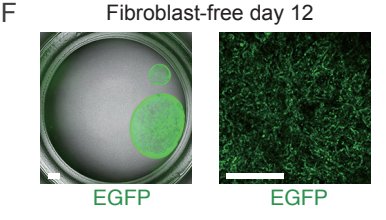
F
Fibroblast-free day 12
EGFP
EGFP

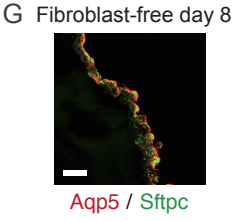
G
Fibroblast-free day 8
Aqp5 / Sftpc

Figure S6. Purification of AEC2 and generation of fibroblast-free alveolospheres, related to Figure 6. (A) Gating scheme for purification of type 2 alveolar epithelial cells and purity of (Lin/CD24/CD34/Sca1)$^{-}$ MHCII^{+} Epcam^{+} cells after cell sorting. Lin: CD31, CD45, Pdgfra, CD146, and Ter119. (B, C) Immunocytochemical analysis of sorted (Lin/CD24/CD34/Sca1)$^{-}$ MHCII^{+} Epcam^{+} population. Sorted cells were labeled with antibodies against Sftpc (B), Krt5, acetylated tubulin, Pdpn, or Scgb1a1 (C). (D) Experimental scheme of the fibroblast-free alveolosphere culture from purified AEC2. (E, F) Representative merged images of representative wells (left; entire Transwell stored in 24-well plates is shown) and confocal micrographs (right) of fibroblast-free alveolosphere cultures on days 8 (E) and 12 (F). (G) Representative section of the fibroblast-free alveolosphere generated from purified AEC2, labeled with antibodies against Aqp5/Sftpc. Scale bars: 25 μm (B, C, G), 500 μm (E, F).

Transparent Methods

Mice.

Female C57BL/6J and C57BL/6-Tg(CAG-EGFP)C14-Y01-FM131Osb (CAG-EGFP) mice (8 weeks of age) were purchased from Japan SLC (Shizuoka, Japan). Col1a2-GFP mice were obtained as previously described (Higashiyama et al., 2009), and were backcrossed to C57BL/6J mice for at least 10 generations before experiments. Fucci mice were obtained as previously described (Niwa et al., 1991; Sakaue-Sawano et al., 2008; Shand et al., 2014). Embryonic day 18.5 (E18.5), postnatal day 0.5 (P0.5), P2, P7, and P28 Col1a2-GFP mice were generated in-house by breeding C57BL/6J with Col1a2-GFP mice. Mice were bred and maintained under specific pathogen-free conditions in the animal facilities at the University of Tokyo and Tokyo University of Science. All experiments were performed in accordance with the guidelines of the Animal Care Committee of the Graduate School of Medicine, the University of Tokyo and Tokyo University of Science.

Murine lung cell preparation.

For preparation of murine lung cells, E18.5, P0.5, P2, P7, P28, and P56 murine lung lobes were collected and minced using a sterile razor. The tissue was dissociated with Dulbecco's Modified Eagle's Medium (DMEM; Sigma-Aldrich) containing 0.96 mg/mL dispase II (Roche), 0.2% collagenase (Wako Pure Chemical Industries), and 20 kU/mL DNase I (Sigma-Aldrich) as previously described (Tsukui et al., 2015). After 60 min incubation at 37°C, the cells were filtered through a 70-μm cell strainer (BD Biosciences) and washed with DMEM supplemented with 2% fetal bovine serum. Erythrocytes were removed by Percoll gradient (70%) centrifugation (GE Healthcare) for 20 min at room temperature (1000 × g).

Antibodies.

Fluorophore- or biotin-conjugated antibodies and streptavidin were purchased from BD Biosciences, BioLegend, Miltenyi Biotec, Calbiochem, Santa Cruz Biotechnology, Life Technologies, Abcam, Sigma-Aldrich, R&D Systems, and Upstate Biotechnology. Antibodies used in this study are listed in Table S7.

Cell sorting.

Cell sorting was performed to purify lung epithelial cells and fibroblasts for lung transcriptome analysis, immunocytochemical analysis, the co-culture alveolosphere formation assay, passaging of the co-cultured alveolospheres, quantitative (q)PCR analysis of alveolospheres, and fibroblast-free alveolosphere generation. For transcriptome analysis,

single-cell suspensions of Col1a2-GFP mouse lung cells were first incubated with anti-mouse CD31, CD45, Ter119, CD146, and Epcam antibodies (Table S7) for 20 min at 4°C. They were then labeled with streptavidin-allophycocyanin (20 min, 4°C), followed by incubation with anti-allophycocyanin microbeads (Miltenyi Biotech; 20 min, 4°C). Labeled cells were magnetically separated with an AutoMACS cell separator (Miltenyi Biotech). Finally, lineage (CD31, CD45, Ter119, and CD146)$^-$ propidium iodide$^-$ Epcam$^+$ live epithelial cells and (CD31, CD45, Ter119, and CD146)$^-$ propidium iodide$^-$ GFP$^+$ live fibroblasts were sorted on a MoFlo Astrios cell sorter (Beckman Coulter) or FACSAria II/III flow cytometer (BD Biosciences).

CAG-EGFP and C57BL/6J mice were used for the co-culture alveolosphere formation assays. Single-cell suspensions of C57BL/6J lung cells were first labeled with anti-mouse CD31, CD45, Ter119, Epcam, and Pdgfra antibodies (Table S7). After magnetic negative selection as described above, lineage (CD31, CD45, CD146, Ter119, Epcam)$^-$ propidium iodide$^-$ Pdgfra$^+$ live fibroblasts were sorted. Single-cell suspensions of CAG-EGFP mouse lung cells were labeled with anti-mouse CD31, CD45, Ter119, and Epcam antibodies. After magnetic negative selection, lineage (CD31, CD45, CD146, Ter119)$^-$ propidium iodide$^-$ Epcam$^+$ epithelial cells were sorted. For fibroblast-free alveolosphere formation, anti-mouse Pdgfra antibody was added to the antibody cocktail for the first step of CAG-EGFP mouse lung cell labeling to maximize sorting purity. For qPCR analysis of alveolospheres, EGFP$^+$ propidium iodide$^-$ epithelial cells and EGFP$^-$ propidium iodide$^-$ fibroblasts were sorted.

Serial analysis of gene expression (SAGE) library construction.

E18.5, P0.5, P2, P7, and P28 epithelial cells (10,000 cells) as well as E18.5, P0.5, P2, P7, P28, and P56 fibroblasts were directly sorted in 500 µL cell lysis buffer composed of 100 mM Tris-HCl (pH 7.5), 1% lithium dodecyl sulfate (Sigma-Aldrich), 500 mM lithium chloride, 10 mM EDTA, and 5 mM dithiothreitol (DTT; Thermo Fisher Scientific). Whole transcripts of epithelial cells were amplified using the primers shown in Table S8 as previously described (Huang et al., 2014), with some modifications. Briefly, 0.5 pmol biotin-TEG-adapter-dT25 primers were bound to 20 µL of Dynabeads M270 streptavidin (Thermo Fisher Scientific). Washed beads were added to each cell lysate and incubated for 30 min at room temperature. The beads were resuspended in a solution of 2 mM dNTP in 10 µL of reverse transcription (RT) mix 1 composed of 1× SuperScript (SS)IV buffer (Thermo Fisher Scientific), 2 M betaine (Sigma-Aldrich), 3.2 U/µL RNaseIn Plus (Promega), and 12 mM $MgCl_2$ followed by incubation for 90 s at 70°C and 5 min at 35°C. For the RT reaction, 10 µl of RT mix 2 composed of 10 mM DTT, 1× SSIV buffer, 10 U/µL SSIV (Thermo Fisher Scientific), and 2

M betaine was added followed by incubation for 5 min at 35°C and for 15 min at 50°C. To digest the reverse-transcribed mRNA, 20 µL of RNase H mix composed of 5 mM DTT, 1× first-strand buffer (Life Technologies), and 0.6 U RNase H (Thermo Fisher Scientific) was added followed by incubation for 20 min at 37°C. For polyA-tailing, 20 µL terminal deoxynucleotidyl transferase (TdT) mix composed of 50 mM Tris-HCl (pH 8.0), 1 mM $CoCl_2$ (Roche), 100 mM KCl, 3 mM $MgCl_2$, 0.65 mM dATP (Thermo Fisher Scientific), and 15.2 U/µL TdT (Roche) was added followed by incubation for 2 min at 37°C. The reaction was terminated by adding 5 µL of 0.5 M EDTA. The beads were washed, and 20 µL of second strand synthesis mix composed of 0.4 µM anchored tagging primer and 1× KAPA Hifi ReadyMix (KAPA Biosystems) was added; second strand synthesis was carried out with the following program: 95°C for 2 min, 98°C for 20 s, 44°C for 2 min, and 72°C for 7 min. The beads were washed, and the first round of whole-transcript amplification (WTA) was performed with 25 µL first WTA mix composed of 0.4 µM 3' WTA primer, 1× KAPA Hifi ReadyMix, and 0.4 µM anchored tagging primer with the following program: 95°C for 3 min; seven cycles of 98°C for 20 s, 65°C for 15 s, and 72°C for 7 min; and 72°C for 5 min. The PCR product was purified with AmPure XP beads (Beckman Coulter). The second WTA mix composed of 0.614 µM biotin-TEG-3' WTA primer, 0.614 µM 5' WTA primer, and 1× KAPA Hifi ReadyMix was added, and the second round of WTA was performed with the following program: 95°C for 3 min; nine cycles of 98°C for 20 s, 65°C for 15 s, and 72°C for 7 min; and 72°C for 5 min. The PCR product was purified using AmPure XP beads.

The SAGE library was constructed as previously described (Matsumura et al., 2012), with some modifications. Briefly, 100 ng of the whole-transcript library was digested with NlaIII (New England Biolabs) for 2 h at 37ºC, and biotinylated 3'-tail transcripts were immobilized to Dynabeads M-280 streptavidin (Thermo Fisher Scientific). Next, 10 pmol of CS1-EcoP15I-NlaIII adapter was ligated for 30 min at 16°C using the Mighty Mix DNA ligation kit (Takara Bio). The beads were resuspended in 200 µL of EcoP15I digestion mix composed of 0.2 U EcoP15I (New England Biolabs), 1× NEBuffer 3.1, and 1 mM ATP and digested for 16 h at 37°C. End repair/A-tailing/ligation reactions were performed by using NEBNext Ultra II modules (New England Biolabs) and 1.875 pmol of CS2-adapter according to the manufacturer's instructions. A MinElute Column (Qiagen) was used to purify the reaction and elution was performed with 13 µL of nuclease-free water. For barcoding, 14.25 µL of a mixture composed of 0.614 µM Ion-trP1-CS2 primer, 1× KAPA Hifi ReadyMix, and 0.614 µM IonA-BC[N]-CS1-primer was combined with 10.75 µL of eluate, and PCR was performed using the following program: 98°C 45 s; nine cycles of 98°C for 15 s, 65°C for 30 s, and 72°C for 90 s; and 72°C for 1 min. Library concentration was quantified using the

KAPA Library Quantification Kit for Ion Torrent (KAPA Biosystems). SAGE libraries were pooled and the concentration was adjusted to 100 pM.

SAGE library sequencing and analysis.

RNA sequencing was performed for two samples of E18.5, P0.5, P2, P7, and P28 epithelial cells and E18.5, P0.5, P2, P7, and P28 fibroblasts obtained from two Col1a2-GFP mice. One sample was sequenced for P56 fibroblasts. Ion Hi-Q Chef Kit, Ion PI v3 Chip kits, and an Ion Proton Sequencer (Thermo Fisher Scientific) were used according to the manufacturer's instructions. Fastq files were evaluated for Q20 ratio using the FastQC (https://www.bioinformatics.babraham.ac.uk/projects/fastqc/) and trimmed using Trimommatic-0.33 (Bolger et al., 2014) and PRINSEQ-0.20.4 (Schmieder and Edwards, 2011). Trimmed reads were mapped to Refseq mm10 using Bowtie2-2.2.5 (Langmead and Salzberg, 2012) with the following parameters: -t -p 11 -N 1 -D 200 -R 20 -L 20 -i S,1,0.50 --norc. Tag numbers representing the expression level of each gene were therefore used as count data. Sample-to-sample normalization was performed with R v.3.4.0 (https://cran.r-project.org/) and TCC package (Sun et al., 2013). Normalized data were then examined for differentially expressed genes (DEGs) using TCC package, which integrates edgeR package (Robinson and Oshlack, 2010) and the glmLRT formula with Benjamini-Hockberg correction. Genes with adjusted $P < 0.05$ and maximum expression > 50 were identified as statistically significant DEGs. These were clustered using the CLICK method (Sharan et al., 2003). Heatmaps were generated in R. Gene Ontology and KEGG pathway enrichment analysis were performed using DAVID (Huang et al., 2009).

For fibroblast ligand–epithelial receptor interactome analysis, fibroblast genes (> 20 tags) annotated with Gene Ontology "extracellular space" and epithelial genes (> 20 tags) annotated with "cell surface receptor" were extracted. Ligand-receptor pathway data were extracted from the KEGG database (Kanehisa et al., 2017) using KEGGgraph (Zhang and Wiemann, 2009) and Pathview package (Luo and Brouwer, 2013) in R v.3.4.0, and fibroblast as well as epithelial cell genes were collated to pathway data. For epithelial–fibroblast, fibroblast–fibroblast, and epithelial–epithelial interactome analyses, fibroblast genes (> 20 tags) with Gene Ontology "cell surface receptor" and epithelial cell genes (> 20 tags) with Gene Ontology "extracellular space" were extracted and collated to pathway data. The temporal pattern of expression data of selected genes was examined for statistical significance among time points using TCC package (Sun et al., 2013).

To calculate correlations between CLICK-identified gene clusters, cluster expression profiles from E18.5 to P56 were summarized by means of the Z-scaled log2 expression value

of each gene. Since there was only one P56 fibroblast sample, expression profiles of P56 epithelial cells were averaged before Z-scaling in order to reduce the number of dimensions used for calculations. To calculate correlations between fibroblast-derived ligands and epithelial-derived receptors, each of their log2 temporal expression profiles were Z-scaled. Pearson's correlation coefficient between cluster means and the associated Student asymptotic P value was calculated by using cor and corPvalueFisher functions of Weighted Co-expression Network Analysis package (Langfelder and Horvath, 2008).

Sequencing of E13.5, E15.5, P14, and P56 epithelial cells of C57BL/6J mice was done similarly and will be detailed elsewhere (n = 2 animals for P56 epithelial cells, and n = 1 for E13.5, E15.5, and P14 epithelial cells). Standardized RNA sequencing data of lung mesenchymal subpopulations (Axin2^{+} Pdgfra^{+}, Axin2^{+} Pdgfra^{-}, and Axin2^{-} Pdgfra^{+} populations sorted from 6- to 8-week-old Axin2CreERT2:tdT:PdgfraEGFP mice (Zepp et al., 2017)) were downloaded from the NCBI Gene Expression Omnibus (GEO; http://www.ncbi.nlm.nih.gov/geo; GSE92699).

Lung alveolosphere formation assay.

For the co-culture alveolosphere formation assay, 5×10^3 epithelial cells derived from 8- to 12-week-old CAG-EGFP mouse lungs and 1×10^5 fibroblasts derived from 8- to 12-week-old C57BL/6J mouse lungs were sorted and collected in 500 µL mouse tracheal epithelial cell (MTEC)/Plus medium (Barkauskas et al., 2013) composed of DMEM/F-12 (Sigma-Aldrich), mouse epidermal growth factor (25 ng/mL; R&D Systems), bovine pituitary extract (30 µg/mL; Sigma-Aldrich), insulin-transferrin-selenium (1×; Thermo Fisher Scientific), penicillin/streptomycin (1×; Sigma-Aldrich), cholera toxin (100 ng/mL; Sigma-Aldrich), and fetal bovine serum (5%). Sorted cells were resuspended in MTEC/Plus medium and mixed at a 1:1 ratio with growth factor-reduced Matrigel (BD Biosciences); 90 µl of the mixture was placed in a 24-well 0.4-µm Transwell clear insert (Falcon; BD Biosciences) (Barkauskas et al., 2013). After Matrigel polymerization (30 min, 37°C), 500 µL MTEC/Plus medium was added to the lower chamber, and the medium was replaced every other day (Barkauskas et al., 2013). Y-27632 Rho kinase inhibitor (10 µM; Wako Pure Chemical Industries) was added to the medium for the first 2 days. For passaging, spheres (culture day 14) were dissociated from the Matrigel with 3 mg/mL dispase II in phosphate-buffered saline (PBS; 60 min, 37°C) (McQualter et al., 2013), washed with PBS, and further incubated with 0.05% trypsin-EDTA for 5 min at 37°C to obtain a single-cell suspension. The 5×10^3 propidium iodide^{-} EGFP^{+} cells were sorted and plated with freshly sorted 1×10^5 fibroblasts derived from C57BL/6J mouse lungs.

Alveolospheres were treated with the following fibroblast ligands and inhibitors: mBmp4 (50 ng/mL), mNoggin (100 ng/mL), mBmp5 (50 ng/mL), hTGF-β1 (20 ng/mL), mFgf2 (250 ng/mL), mFgf7 (100 ng/mL), and hFGF10 (100 ng/mL) (all from R&D Systems); SB431542 (10 μM; Sigma-Aldrich); and CHIR99021 (3 μM; Wako Pure Chemical Industries). These were added to the culture medium on day 2 of culture (at the time of the first medium change) and thereafter. Images were acquired after 14 days of culture with an SP-5 confocal microscope (Leica Microsystems) or BZ-9000/BZ-X800 digital microscope (Keyence). Gamma correction ($\gamma = 1.3$) was performed for images obtained with the BZ-9000 microscope. For the proliferation assay, 5×10^3 epithelial cells derived from 8- to 12-week-old Fucci mouse lungs and 1×10^5 fibroblasts derived from 8- to 12-week-old C57BL/6J mouse lungs were plated and treated with the ligands and inhibitors on days 1 and 3 of culture and analyzed on day 4 or 5. Spheres were dissociated from the Matrigel with Cell Recovery Solution (Sigma-Aldrich) according to manufacturer's protocol and were analyzed by flow cytometry.

For fibroblast-free alveolospheres formation assay, 5×10^3 epithelial cells derived from 8- to 12-week old CAG-EGFP mouse lungs were sorted in 500 μL of MTEC/Plus medium, resuspended in the MTEC/Plus medium, and mixed at a 1:1 ratio with growth factor-reduced Matrigel containing Jagged-1 peptide (1 μM; AnaSpec). After Matrigel polymerization, 500 μL MTEC/Plus medium containing mNoggin (100 ng/mL), SB431542 (10 μM), CHIR99021 (3 μM), mFgf7 (100 ng/mL), and heparin sodium salt (100 ng/ml; Sigma-Aldrich) were added to the lower chamber. To assess the contribution of Notch signaling, the γ-secretase inhibitor DAPT (10 mM; Sigma-Aldrich) or dimethylsulfoxide (Sigma-Aldrich) was used. The medium was changed every other day with the same medium that also containing Jagged-1 (1 μM). For passaging, spheres were suspended using dispase or Cell Recovery Solution, and cells filtered through a 70-μm cell strainer were transferred to fresh Matrigel containing Jagged-1. A total of 2×10^3–5×10^3 cells were passaged every 8–12 days. Images were acquired after 8–12 days of culture. Colony size and number were quantified using ImageJ v.1.8 (National Institutes of Health; http://imagej.nih.gov/ij). Colony-forming efficiency was defined as the number of colonies formed divided by the number of cells plated.

Real-time qPCR analysis.

The qPCR analysis was performed using Thunderbird SYBR qPCR Mix (Toyobo, Osaka, Japan) for detection of amplified cDNA on an ABI 7500 real-time PCR system (Life Technologies). A portion of the cDNA obtained from SAGE analysis or the alveolosphere

formation assay was used as the template. mRNA levels were normalized to that of *Gapdh* or *Actb* in each sample. Primers used for qPCR are shown in Table S8. Primer sequences for *Fgfr1c* (Williamson et al., 2012), *Fgfr2b* (Vandanmagsar et al., 2016), and fibroblast-associated genes (Tsukui et al., 2015) have been previously reported.

Immunohistochemistry and immunocytochemistry.

Immunohistochemical analysis of lungs was performed as previously described (Tsukui et al., 2013). The alveolospheres were centrifuged at 100 × g for 1 min and collected using iPGell (GenoStaff). The spheres were fixed with 4% paraformaldehyde in PBS for 30 min at room temperature, soaked overnight in 30% sucrose, and embedded in Optimal Cutting Temperature compound (Sakura Finetek Japan), and cryosections (10 μm in thickness) were prepared. Antibodies used are listed in Table S7. Images were acquired with an SP-5 confocal microscope.

The sorted cells were prepared for immunocytochemical analysis using Smear Gell (GenoStaff). After fixing with 4% paraformaldehyde in PBS for 30 min at room temperature, the cells were stained with the antibodies listed in Table S7.

Flow cytometry.

For the flow cytometric analysis of Col1a2-GFP mouse lungs and co-cultured alveolospheres, single-cell suspensions of lungs or alveolospheres were collected as described. Flow-Count Fluorospheres (Beckman Coulter) were used to estimate cell numbers. Single-cell suspensions were blocked with anti-CD16/32 monoclonal antibody (BioLegend) for incubation for 15 min at 4°C, and stained for 30 min at 4°C with the antibodies listed in Table S7. Data were acquired on a Gallios flow cytometer (Beckman Coulter) and analyzed with FlowJo software (version 10.4.1; FlowJo LLC).

Statistical analyses.

Data from qPCR analyses and for organoid size are shown as mean ± standard error. Differences between means of measurements were evaluated with the unpaired Student's *t* test (two-tailed). Differences in the means of more than two groups were assessed by one-way analysis of variance (ANOVA) with Tukey-Kramer's multiple comparisons *post-hoc* test. $P < 0.05$ was considered statistically significant. Statistical analyses were performed with a GraphPad Prism v.5.01 software (GraphPad Inc.).

Data and Software Availability.

Raw data from RNA sequencing have been deposited in the GEO. The GEO accession number for the RNA sequencing data of epithelial cells and fibroblasts from Col1a2-GFP mice reported in this paper is GSE113160 and RNA sequencing data of E13.5, E15.5, P14, and P56 epithelial cells from C57BL/6J mice is GSE109847.

Supplemental References

Barkauskas, C.E., Cronce, M.J., Rackley, C.R., Bowie, E.J., Keene, D.R., Stripp, B.R., Randell, S.H., Noble, P.W., and Hogan, B.L.M. (2013). Type 2 alveolar cells are stem cells in adult lung. J. Clin. Invest. 123, 3025–3036.

Bolger, A.M., Lohse, M., and Usadel, B. (2014). Trimmomatic: a flexible trimmer for Illumina sequence data. Bioinformatics 30, 2114–2120.

Higashiyama, R., Moro, T., Nakao, S., Mikami, K., Fukumitsu, H., Ueda, Y., Ikeda, K., Adachi, E., Bou-Gharios, G., Okazaki, I., et al. (2009). Negligible contribution of bone marrow-derived cells to collagen production during hepatic fibrogenesis in mice. Gastroenterology 137, 1459–66.e1.

Huang, D.W., Sherman, B.T., and Lempicki, R.A. (2009). Systematic and integrative analysis of large gene lists using DAVID bioinformatics resources. Nat. Protoc. 4, 44–57.

Huang, H., Goto, M., Tsunoda, H., Sun, L., Taniguchi, K., Matsunaga, H., and Kambara, H. (2014). Non-biased and efficient global amplification of a single-cell cDNA library. Nucleic Acids Res. 42, e12–e12.

Kanehisa, M., Furumichi, M., Tanabe, M., Sato, Y., and Morishima, K. (2017). KEGG: new perspectives on genomes, pathways, diseases and drugs. Nucleic Acids Res. 45, D353–D361.

Langfelder, P., and Horvath, S. (2008). WGCNA: an R package for weighted correlation network analysis. BMC Bioinformatics 9, 559.

Langmead, B., and Salzberg, S.L. (2012). Fast gapped-read alignment with Bowtie 2. Nat. Meth. 9, 357–359.

Luo, W., and Brouwer, C. (2013). Pathview: an R/Bioconductor package for pathway-based data integration and visualization. Bioinformatics 29, 1830–1831.

Matsumura, H., Urasaki, N., Yoshida, K., Krüger, D.H., Kahl, G., and Terauchi, R. (2012). SuperSAGE: powerful serial analysis of gene expression. Methods Mol. Biol. 883, 1–17.

McQualter, J.L., McCarty, R.C., Van der Velden, J., O'Donoghue, R.J.J., Asselin-Labat, M.-L., Bozinovski, S., and Bertoncello, I. (2013). TGF-β signaling in stromal cells acts upstream of FGF-10 to regulate epithelial stem cell growth in the adult lung. Stem Cell Res. 11, 1222–1233.

Niwa, H., Yamamura, K., and Miyazaki, J. (1991). Efficient selection for high-expression transfectants with a novel eukaryotic vector. Gene 108, 193–199.

Robinson, M.D., and Oshlack, A. (2010). A scaling normalization method for differential expression analysis of RNA-seq data. Genome Biol. 11, R25.

Sakaue-Sawano, A., Kurokawa, H., Morimura, T., Hanyu, A., Hama, H., Osawa, H., Kashiwagi, S., Fukami, K., Miyata, T., Miyoshi, H., et al. (2008). Visualizing spatiotemporal dynamics of multicellular cell-cycle progression. Cell 132, 487–498.

Schmieder, R., and Edwards, R. (2011). Quality control and preprocessing of metagenomic datasets. Bioinformatics 27, 863–864.

Shand, F.H.W., Ueha, S., Otsuji, M., Koid, S.S., Shichino, S., Tsukui, T., Kosugi-Kanaya, M., Abe, J., Tomura, M., Ziogas, J., et al. (2014). Tracking of intertissue migration reveals the origins of tumor-infiltrating monocytes. Proc. Natl. Acad. Sci. U.S.A. 111, 7771–7776.

Sharan, R., Maron-Katz, A., and Shamir, R. (2003). CLICK and EXPANDER: a system for clustering and visualizing gene expression data. Bioinformatics 19, 1787–1799.

Sun, J., Nishiyama, T., Shimizu, K., and Kadota, K. (2013). TCC: an R package for comparing tag count data with robust normalization strategies. BMC Bioinformatics 14, 219.

Tsukui, T., Ueha, S., Abe, J., Hashimoto, S.-I., Shichino, S., Shimaoka, T., Shand, F.H.W., Arakawa, Y., Oshima, K., Hattori, M., et al. (2013). Qualitative rather than quantitative changes are hallmarks of fibroblasts in bleomycin-induced pulmonary fibrosis. Am. J. Pathol. 183, 758–773.

Tsukui, T., Ueha, S., Shichino, S., Inagaki, Y., and Matsushima, K. (2015). Intratracheal cell transfer demonstrates the profibrotic potential of resident fibroblasts in pulmonary fibrosis. Am. J. Pathol. 185, 2939–2948.

Vandanmagsar, B., Warfel, J.D., Wicks, S.E., Ghosh, S., Salbaum, J.M., Burk, D., Dubuisson, O.S., Mendoza, T.M., Zhang, J., Noland, R.C., et al. (2016). Impaired mitochondrial fat oxidation induces FGF21 in muscle. Cell Rep. 15, 1686–1699.

Williamson, I., Eskeland, R., Lettice, L.A., Hill, A.E., Boyle, S., Grimes, G.R., Hill, R.E., and Bickmore, W.A. (2012). Anterior-posterior differences in HoxD chromatin topology in limb development. Development 139, 3157–3167.

Zepp, J.A., Zacharias, W.J., Frank, D.B., Cavanaugh, C.A., Zhou, S., Morley, M.P., and Morrisey, E.E. (2017). Distinct mesenchymal lineages and niches promote epithelial self-renewal and myofibrogenesis in the lung. Cell 170, 1134–1148.e10.

Zhang, J.D., and Wiemann, S. (2009). KEGGgraph: a graph approach to KEGG PATHWAY in R and bioconductor. Bioinformatics 25, 1470–1471.